

The Galaxy Clustering Crisis in Abundance Matching

Duncan Campbell^{1*}, Frank C. van den Bosch¹, Nikhil Padmanabhan^{2,3}, Johannes Lange¹, Yao-Yuan Mao⁴, Fangzhou Jiang⁵, Antonio Villarreal⁴, and Andrew Zentner⁴

¹Department of Astronomy, Yale University, New Haven, CT 06511, USA

²Department of Physics, Yale University, New Haven, CT 06520, USA

³Yale Center for Astronomy and Astrophysics, Yale University, New Haven, CT 06520, USA

⁴Department of Physics and Astronomy & Pittsburgh Particle Physics, Astrophysics, and Cosmology Center (PITT PACC), University of Pittsburgh, Pittsburgh, PA 15260

⁵Racah Institute of Physics, The Hebrew University, Jerusalem 91904, Israel

Accepted XXX. Received YYY; in original form ZZZ

ABSTRACT

Galaxy clustering on small scales is significantly under-predicted by sub-halo abundance matching (SHAM) models that populate (sub-)haloes with galaxies based on peak halo mass, M_{peak} . SHAM methods based on the peak maximum circular velocity, V_{peak} , have had much better success. The primary reason M_{peak} based models fail is the relatively low abundance of satellite galaxies produced in these models compared to those based on V_{peak} . Despite success in predicting clustering, a simple V_{peak} based SHAM model results in predictions for galaxy growth that are at odds with observations. We evaluate three possible remedies that could “save” mass-based SHAM. 1.) SHAM models require a significant population of “orphan” galaxies as a result of artificial disruption/merging of sub-haloes in modern high resolution dark matter simulations, 2.) satellites must grow significantly after being accretion, and/or 3.) stellar mass is significantly affected by halo assembly history. Regardless of the particulars, we show that popular SHAM models based on M_{peak} cannot be correct as presented. Either V_{peak} truly is a better predictor of stellar mass, or SHAM models are missing vital component(s) that significantly affect galaxy clustering.

Key words: galaxies: halos – galaxies: evolution – galaxies: clustering

1 INTRODUCTION

The prevailing picture of galaxy formation is intricately tied to that of dark matter structure formation. The matter distribution of the Universe evolved from a relatively smooth state into a complex web of structure over ~ 14 billion years. Within this web, small inhomogeneities evolved into extended, quasi-spherical, gravitationally bound objects called haloes. The build-up of structure proceeds hierarchically as smaller haloes are accreted into larger haloes, becoming substructures called sub-haloes. The potential wells of dark matter (sub-)haloes are the natural site for galaxies to form as baryons cool and condense into stars (Rees & Ostriker 1977; White & Rees 1978; Fall & Efstathiou 1980).

This general, albeit coarse, view of galaxy formation fits well with the premise of sub-halo abundance matching (SHAM). SHAM in its most simple form rests on the hypoth-

esis that all massive¹ (sub-)haloes host galaxies, all galaxies occupy (sub-)haloes, and there is a simple monotonic relation between galaxy mass and the mass of the (sub-)halo each galaxy occupies (Kravtsov et al. 2004; Conroy et al. 2006; Vale & Ostriker 2004). This approach relies on simulations of dark matter structure formation to provide robust statistical predictions for many properties of dark matter (sub-)haloes, e.g. halo mass functions, mass profiles, and the spatial clustering of haloes. By “populating” dark matter simulations with galaxies using the SHAM technique, the statistical predictions from simulations can be leveraged to constrain the galaxy-halo connection and make predictions for how galaxies form and evolve along with (sub-)haloes.

The stellar mass-halo mass (SMHM) relation is one of the most fundamental implications of SHAM. The SMHM relation at redshift ~ 0 inferred using SHAM is consistent

* E-mail: duncan.campbell@yale.edu

¹ above a limiting lower mass scale below which galaxy formation becomes inefficient

with HOD/CLF analysis (Yang et al. 2003; van den Bosch et al. 2003, 2007; Yang et al. 2013; Zu & Mandelbaum 2015a) and independent, more direct, measurements, e.g. galaxy-galaxy lensing, satellite kinematics, and the Tully-Fisher relation (Wang et al. 2006; More et al. 2009; Guo et al. 2010; Wang & Jing 2010; Moster et al. 2010; Behroozi et al. 2010; Mandelbaum et al. 2015; Desmond & Wechsler 2015; van Uitert et al. 2016). By extending this analysis to higher redshifts, the inferred evolution of the SMHM relation and the mass growth histories of haloes predicted by simulations provide constraints on the average stellar mass growth histories of galaxies that is consistent with the cosmic star-formation history of the Universe (Conroy & Wechsler 2009; Wang & Jing 2010; Yang et al. 2012; Moster et al. 2013; Behroozi et al. 2013c). An important finding of these studies is that the peak in star-formation efficiency shifts towards more massive haloes at earlier times.

The ability of SHAM to accurately predict the clustering of galaxies is more limited. In particular, the small scale clustering of galaxies remains difficult to fit. SHAM has only been shown to be consistent with galaxy clustering under one of two conditions: 1.) stellar mass is tied to the peak circular velocity of (sub-)haloes (or closely related quantities) (Reddick et al. 2013; Hearin et al. 2014; Lehmann et al. 2015), or 2.) the abundance of sub-haloes is treated as a free parameter (Wang et al. 2006; Wang & Jing 2010; Guo et al. 2010; Moster et al. 2010; Yang et al. 2012). This second approach relies on a population of “orphan” galaxies which have no identifiable sub-halo in a simulation. As we will show in this work, both of these assumptions are problematic. The assumption that stellar mass should be better correlated with maximum circular velocity over halo mass has not been robustly motivated. Furthermore, we show that models that make this assumption are at odds with previous work on the evolution of the SMHM relation. Orphan galaxies are difficult to reconcile with modern high resolution dark matter simulations which aim to resolve substructure. We summarize this state of affairs in Fig. 1. There is no published SHAM model which fits both galaxy clustering and the evolution of the stellar mass function using resolved substructure in a dark matter simulation without the addition of “orphan” galaxies.

The goal of this paper is threefold: to make explicit the tension between fitting galaxy clustering measurements and the evolution of the stellar mass function within the SHAM framework, to examine the successes and failures of SHAM models based on maximum circular velocity, and to evaluate mechanisms to alleviate the clustering crisis in models based on halo mass. The models and analysis in this paper utilize the framework and code base in `Halotools` (Hearin et al. 2016), an `Astropy` (The Astropy Collaboration et al. 2013) affiliated Python² package. We also make available all of the code and data products necessary to reproduce the figures and analysis in this paper³. Throughout, we scale all units by $h = H_0/[100 \text{ km/s Mpc}^{-1}]$ where appropriate, and we use $\log(x)$ to indicate the base 10 logarithm of x .

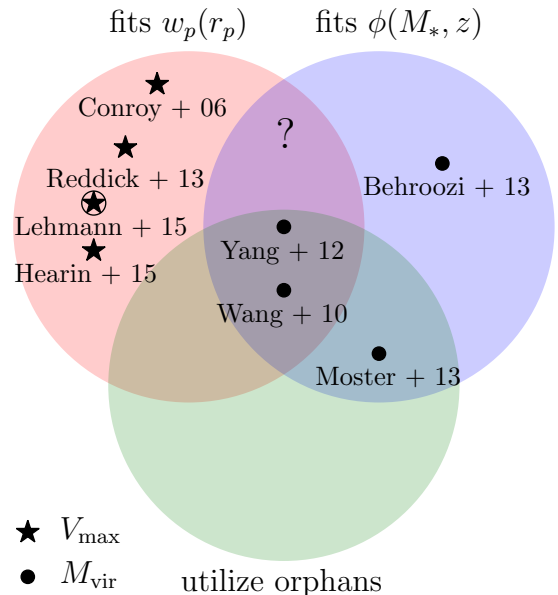


Figure 1. Venn diagram of selected SHAM models within three sets; those that fit the galaxy clustering, $w_p(r_p)$ (upper left red region), those that fit the evolution of the galaxy stellar mass function, $\phi(M_*, z)$ (upper right blue region), and those that utilize orphan galaxies (lower green region). Models marked with a circle are based on measures of halo mass, M_{vir} , including peak quantities. Models marked with a star are based on measures of halo maximum circular velocity, V_{\max} , including peak quantities, with the Lehmann et al. (2015) model falling somewhere in between. This paper focuses on the lack of models in the region marked with a “?”.

2 METHODS

2.1 Abundance Matching Models

SHAM, in its most simple form, assumes that the cumulative abundance of galaxies and haloes can be used to map galaxy properties uniquely onto (sub-)haloes. Using stellar mass, M_* , and a halo mass proxy \mathcal{M} , SHAM assumes:

$$N(> M_*) = N(> \mathcal{M}) \implies M_* = f(\mathcal{M}) \quad (1)$$

where $f(\mathcal{M})$ is some monotonically increasing function. This maps the most massive galaxies to the most massive haloes. The function $f(\mathcal{M})$ may be determined non-parametrically by matching the rank orders of galaxies and haloes. We refer to this method of SHAM as “rank order” abundance matching. However, we also consider another class of SHAM models where $f(\mathcal{M})$ is parametrized. This introduces the possibility that the observed abundance of galaxies is not strictly matched; however, it is generally the goal of such models to preserve this characteristic. We consider these two types of models similar enough to be contained within the class of models we refer to as SHAM.

The predictions of SHAM are sensitive to the details of how it is implemented. Many halo properties have been examined in search of which “best” correlates with galaxy stellar mass or luminosity. It is generally found that “peak” values of mass-like properties, estimated over the history of the (sub-)halo, work best. Specifically, using the peak maxi-

² <http://www.python.org>

³ https://github.com/duncandc/Clustering_Crisis

113 mum circular velocity reproduces the clustering statistics of
 114 galaxies most successfully (Conroy et al. 2006; Reddick et al.
 115 2013). The difference between the peak values and current
 116 values is most pronounced for sub-haloes, as sub-haloes are
 117 subject to stripping processes which remove mass, while the
 118 core of the sub-halo, which hosts a galaxy, is thought to sur-
 119 vive much longer (e.g. Behroozi et al. 2014a; van den Bosch
 120 et al. 2016; Jiang & van den Bosch 2016; van den Bosch &
 121 Jiang 2016, and references therein). Implicit to the SHAM
 122 algorithm is that the processes that set the properties of
 123 central and satellite galaxies are independent of halo assem-
 124 bly history. This assumption has been relaxed somewhat by
 125 allowing satellites to either grow or lose stellar mass after
 126 being accreted into a host-halo (Watson et al. 2012; Yang
 127 et al. 2012; Behroozi et al. 2015) and is well motivated by
 128 observations (Wetzel et al. 2013). Furthermore, the very dis-
 129 tinction between host-haloes and sub-haloes is blurred by
 130 the recognition that some haloes are accreted into a host-
 131 halo, only for their orbit to take them outside their host’s
 132 virial radius. For these “backsplash” haloes, it may be more
 133 appropriate to treat them as sub-haloes likely to host galax-
 134 ies that have properties more in common with traditionally
 135 defined satellite galaxies (Mamon et al. 2004; Wetzel et al.
 136 2014).

137 Below, we review a set of SHAM models and our method
 138 of implementing each before examining the clustering pre-
 139 dictions of each model in the following section. We provide
 140 a summary of the models used in this paper in table 1.

141 2.1.1 Rank Order SHAM

142 The simplest implementation of SHAM maps galaxies into
 143 (sub-)haloes by matching rank orders. Given a set of galax-
 144 ies, $M_* = \{M_{*i}\}$, and (sub-)haloes, $\mathcal{M} = \{\mathcal{M}_j\}$, of the same
 145 size, this method proceeds by calculating the ranks of each:

$$146 \quad n_i^{\text{gal}} = \mathcal{R}(M_*) \\ 147 \quad n_j^{\text{halo}} = \mathcal{R}(\mathcal{M}) \quad (2)$$

148 where the $\mathcal{R}()$ function returns the ordinal ranks. Each
 149 galaxy is then assigned to a (sub-)halo with the equivalent
 150 rank, i.e. $n_i^{\text{gal}} = n_j^{\text{halo}}$. We consider two rank order SHAM
 151 models in this paper, one based on M_{peak} and one on V_{peak} .
 152 As shorthand, we refer to these models as “RM” and “RV”,
 153 respectively.

154 Given a set of galaxies and haloes, this mapping is deter-
 155 ministic. However, the assumption of perfect rank ordering
 156 with respect to the cumulative distribution can be relaxed,
 157 allowing for stochasticity in the mapping and resulting in
 158 a probabilistic relation between stellar mass and halo mass,
 159 $P(M_*|\mathcal{M})$. There are various methods used in the literature
 160 to add scatter to this relation while maintaining agreement
 161 with an observed stellar mass function. One may attempt to
 162 deconvolve the stellar mass function from the scatter model
 163 such that, after solving for eq. (1) with this deconvolved
 164 function and applying the scatter model, the new stellar
 165 mass function is consistent with the observed function (e.g.
 166 Behroozi et al. 2010). Another option is to manually add
 167 scatter to the stellar masses used in abundance matching,
 168 re-ranking on the new values to perform the matching, and
 169 iteratively solving for a solution that results in the desired
 170 amount of scatter in the SMHM relation (e.g. Hearin et al.

Table 1. Summary SHAM models used in this paper

name	reference	description
RM	–	rank order SHAM on M_{peak}
RV	–	rank order SHAM on V_{peak}
M13	Moster et al. (2013)	evolving SMHM model
B13	Behroozi et al. (2013c)	evolving SMHM model
Y12	Yang et al. (2012)	evolving SMHM model

171 2013). A third option is to parametrize the SMHM relation
 172 and fit for the parameters which result in a stellar mass
 173 function that is consistent with an observed function after
 174 populating a dark matter simulation. We will examine this
 175 type of model in the following sections.

176 We do not go through the additional step of adding scatter
 177 to our RM and RV models, as scatter in the SMHM relation
 178 generally decreases the strength of the clustering signal
 179 for massive galaxies ($M_* > 10^{11} h^{-2} M_\odot$) with little effect
 180 at lower masses (Tinker et al. 2016), and this work focuses
 181 on the decrement in galaxy clustering signal for samples of
 182 less massive galaxies in SHAM models.

183 2.1.2 Moster et al. (2013) SHAM

184 Moster et al. (2013) parametrize the SMHM relation as a
 185 function of halo mass and redshift to account for evolution.
 186 Furthermore, they assume the stellar mass of satellite galax-
 187 ies is determined by the mass of the sub-halo at the time of
 188 its accretion into a more massive host-halo for the first time.
 189 The functional form is given by:

$$\frac{\langle M_* | \mathcal{M} \rangle_{\text{med}}(a)}{\mathcal{M}} = 2N \left[\left(\frac{\mathcal{M}}{M_1} \right)^{-\beta} + \left(\frac{\mathcal{M}}{M_1} \right)^\gamma \right]^{-1} \quad (3)$$

190 where $\langle \rangle_{\text{med}}$ indicates the median. The evolution of the pa-
 191 rameters is given by:

$$\log[M_1(a)] = M_{10} + M_{11}(1-a) \quad (4)$$

$$N(a) = N_{10} + N_{11}(1-a) \quad (5)$$

$$\beta(a) = \beta_{10} + \beta_{11}(1-a) \quad (6)$$

$$\gamma(a) = \gamma_{10} + \gamma_{11}(1-a) \quad (7)$$

192 where the scale factor is either the instantaneous scale factor,
 193 or the one at the time of accretion:

$$a = \begin{cases} a & \text{if host-halo} \\ a_{\text{acc}} & \text{if sub-halo} \end{cases} \quad (8)$$

194 and \mathcal{M} is the instantaneous mass or the mass at accretion,
 195 M_{acc} , for sub-haloes. Scatter in the SMHM relation is mod-
 196 elled as a fixed log-normal with $\sigma_{\log(M_*)} \approx 0.18$.

197 Moster et al. (2013) find the best fit parameters for
 198 equation (3) that reproduce the stellar mass function at var-
 199 ious redshifts between 0 and ~ 4 . They also show that the
 200 implied star-formation rates of galaxies given the growth
 201 history of the (sub-)haloes in their simulation is consistent
 202 with the cosmic star-formation rate density. The parame-
 203 ters were constrained using the Millennium simulation with
 204 (sub-)haloes defined as spherical over-densities (SO) with
 205 mean internal density 200 times the critical density of the
 206 universe, M_{200c} . As shorthand, we will refer to this model as

“M13”. The parameter values used in this paper are taken directly from Moster et al. (2013) and listed in table 2.

2.1.3 Behroozi et al. (2013) SHAM

Behroozi et al. (2013c) make similar assumptions as M13 but utilize a different parametrization given by:

$$\log[\langle M_* | \mathcal{M} \rangle_{\text{med}}(a)] = \log(\epsilon M_1) + f(\log(\mathcal{M}/M_1)) - f(0) \quad (9)$$

where,

$$f(x) = -\log(10^{\alpha x} + 1) + \delta \frac{[\log(1 + \exp[x])]^\gamma}{1 + \exp(10^{-x})} \quad (10)$$

and where $\mathcal{M} = M_{\text{peak}}$. The parameters evolve with redshift as:

$$\nu(a) = e^{-4a^2} \quad (11)$$

$$\log[M_1(a)] = M_{10} + \nu [M_{1,a}(a-1) + M_{1,z}z] \quad (12)$$

$$\log[\epsilon(a)] = \epsilon_0 + \nu [\epsilon_a(a-1) + \epsilon_z z] + \epsilon_{a,2}(a-1) \quad (13)$$

$$\alpha(a) = \alpha_0 + \nu [\alpha_a(a-1)] \quad (14)$$

$$\delta(a) = \delta_0 + \nu [\delta_a(a-1) + \delta_z z] \quad (15)$$

$$\gamma(a) = \gamma_0 + \nu [\gamma_a(a-1) + \gamma_z z] \quad (16)$$

When fitting their model, Behroozi et al. (2013c) also allow the scatter in the SMHM relation to vary as a function of redshift. The variation found is consistent with no variation (constant over cosmic time), so we neglect the small variation in the best fit model and use a constant non-varying scatter. We have checked that including this variation has no appreciable effect on our conclusions. As shorthand, we will refer to this model as “B13”. Behroozi et al. (2013c) constrained the parameters of this model by fitting the stellar mass function at multiple epochs, specific star-formation rates, and the cosmic star-formation history between $z=0$ -8. The values used in this paper are taken directly from Behroozi et al. (2013c) and listed in table 2.

2.1.4 Yang et al. (2012) SHAM

Yang et al. (2012) take a different approach than M13 and B13. They allow for evolution with redshift in a similar manner, but additionally allow satellites to grow or lose mass after the time of accretion. The SMHM relation for central galaxies is:

$$\langle M_{*,\text{cen}} | \mathcal{M} \rangle_{\text{med}}(z) = M_0 \frac{(\mathcal{M}/M_1)^{\alpha+\beta}}{(1 + \mathcal{M}/M_1)^\beta} \quad (17)$$

where $\mathcal{M} = M_{180b}$, and the parameters⁴ evolve with redshift as:

$$\log[M_0(z)] = M_{01} + \gamma_1 z \quad (18)$$

$$\log[M_1(z)] = M_{11} + \gamma_2 z \quad (19)$$

$$\alpha(z) = \alpha_0 + \gamma_3 z \quad (20)$$

$$\log[\beta(z)] = \log(\beta_0) + \gamma_4 z + \gamma_5 z^2 \quad (21)$$

⁴ We have altered the naming scheme somewhat to be more consistent with the other models.

The median stellar mass of satellites is determined by interpolating between the stellar mass a satellite would have had at the time of accretion and the stellar mass of a central galaxy with the same halo mass as the satellite at accretion at redshift, z . This value is determined by a single parameter, c :

$$\langle M_{*,\text{sat}}(z, z_{\text{acc}}) \rangle = (1 - c) \langle M_{*,\text{cen}} | \mathcal{M}_{\text{acc}} \rangle(z_{\text{acc}}) + c \langle M_{*,\text{cen}} | \mathcal{M} \rangle(z) \quad (22)$$

where \mathcal{M}_{acc} is the halo mass proxy at the time of accretion for the sub-halo. The case where $c = 0$ corresponds to no growth (or mass loss) since z_{acc} . The case where $c = 1$ corresponds to using the same SMHM relation for centrals and satellites at all redshifts.

Apart from the parametrization of the SMHM relation and its evolution, the original implementation of Yang et al. (2012) differs significantly from the previous two models in that it uses a fully analytical halo+sub-halo model for abundances, sub-halo profiles, and halo bias. We take a different approach and use the SMHM relation of the model and apply it directly to a simulation, side-stepping the need to analytically model these components. Multiple fits were performed in Yang et al. (2012). We use the parameter constraints determined by fitting the stellar mass function at multiple epochs ($z=0$ -5) as well as the conditional stellar mass function at $z \sim 0$. This set of parameters was also shown to fit galaxy clustering observations well at $z \sim 0$. The values used in this paper are listed in table 2, specifically these are taken from Table 4 (ID=4) in Yang et al. (2012). As shorthand, we will refer to this model as “Y12”.

2.2 Dark Matter Simulations

We build mock galaxy catalogues using the 5 SHAM models described in the preceding sections using the Bolshoi (Klypin et al. 2011) simulation output at $z = 0$. The Bolshoi simulation follows the evolution of 2048³ dark matter particles using the Adaptive Refinement Tree (ART) code (Kravtsov, Klypin & Khokhlov 1997) in a flat Λ CDM cosmology with parameters $\Omega_{\text{m},0} = 1 - \Omega_{\Lambda,0} = 0.27$, $\Omega_{\text{b},0} = 0.0469$, $n_s = 0.95$, $\sigma_8 = 0.82$, and $h = 0.7$ (hereafter “Bolshoi cosmology”). The box size of the Bolshoi simulation is $L_{\text{box}} = 250 h^{-1} \text{Mpc}$, with a dark matter particle mass of $m_{\text{p}} = 1.35 \times 10^8 h^{-1} \text{M}_\odot$.

(Sub-)haloes are found using the phase-space halo finder ROCKSTAR (Behroozi et al. 2013a,b), which uses adaptive, hierarchical refinement of friends-of-friends groups in six phase-space dimensions and one time dimension. As demonstrated in Knebe et al. (2011, 2013), this results in a very robust tracking of (sub-)haloes (also see van den Bosch & Jiang 2014). Haloes in this catalogue are defined to be spherical volumes centred on a local density peak (SO hereafter), such that the average density inside the sphere is $\bar{\rho}_{\text{h}}(z) = \Delta_{\text{vir}}(z)\rho_{\text{m}}(z)$. Here $\rho_{\text{m}}(z) = \Omega_{\text{m}}(z)\rho_{\text{crit}}(z)$, where $\rho_{\text{crit}}(z) = 3H(z)^2/8\pi G$ is the critical energy density of the Universe, and $\Delta_{\text{vir}}(z)$ is given by a fitting function (Bryan & Norman 1998):

$$\Delta_{\text{vir}}(z) = [18\pi^2 - 82\Omega_{\Lambda}(z) - 39\Omega_{\Lambda}^2(z)] \Omega_m^{-1} \quad (23)$$

For the Bolshoi cosmology, $\Delta_{\text{vir}}(z = 0) \simeq 360$. The radius of each such sphere defines the virial radius R_{vir} of the halo, which is related to the mass of the halo via

Table 2. Parameter values used for the evolving SHAM models presented in this paper. Mass parameters in M13 and B13 are scaled to $h=0.7$, while in Y12, $h=1$ as is the practice in the rest of this paper. We use the parameters as is, and scale the output stellar masses to $h=1$.

model	parameter	value	uncertainty
M13	M_{10}	11.590	± 0.236
M13	M_{11}	1.195	± 0.353
M13	N_{10}	0.0351	± 0.0058
M13	N_{11}	-0.0247	± 0.0069
M13	β_{10}	1.376	± 0.153
M13	β_{11}	-0.826	± 0.225
M13	γ_{10}	0.608	± 0.059
M13	γ_{11}	0.329	± 0.173
B13	M_{10}	11.514	$\pm^{0.053}_{0.009}$
B13	$M_{1,a}$	-1.793	$\pm^{0.315}_{0.330}$
B13	$M_{1,z}$	-0.251	$\pm^{0.125}_{0.132}$
B13	ϵ_0	-1.777	$\pm^{0.166}_{0.138}$
B13	ϵ_a	-0.006	$\pm^{0.361}_{0.113}$
B13	ϵ_z	-0.000	$\pm^{0.104}_{0.003}$
B13	$\epsilon_{a,2}$	-0.119	$\pm^{0.061}_{0.012}$
B13	α_0	-0.119	$\pm^{0.061}_{0.012}$
B13	α_a	-0.119	$\pm^{0.061}_{0.012}$
B13	δ_0	-1.777	$\pm^{0.133}_{0.146}$
B13	δ_a	-0.006	$\pm^{0.113}_{0.361}$
B13	δ_z	-0.000	$\pm^{0.003}_{0.104}$
B13	γ_0	-1.777	$\pm^{0.138}_{0.166}$
B13	γ_a	-0.006	$\pm^{0.361}_{0.113}$
B13	γ_z	-0.000	$\pm^{0.003}_{0.104}$
Y12	M_{01}	10.36	$\pm^{0.05}_{0.06}$
Y12	M_{11}	11.06	$\pm^{0.08}_{0.15}$
Y12	α_0	0.27	$\pm^{0.01}_{0.01}$
Y12	β_0	4.34	$\pm^{0.96}_{0.52}$
Y12	γ_1	-0.96	$\pm^{0.19}_{0.13}$
Y12	γ_2	-0.23	$\pm^{0.06}_{0.05}$
Y12	γ_3	-0.41	$\pm^{0.07}_{0.08}$
Y12	γ_4	-0.11	$\pm^{0.11}_{0.08}$
Y12	γ_5	0.01	$\pm^{0.05}_{0.07}$
Y12	c	1.0	—

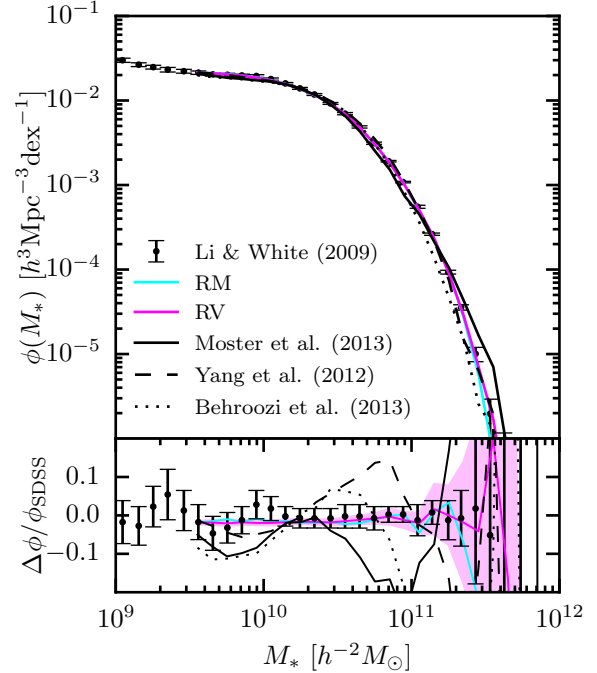


Figure 2. The stellar mass function of a mock realization of each model is plotted (lines). For comparison we show the stellar mass function in SDSS as measured by Li & White (2009) as points with error bars. The lower panel shows the residuals with respect to the triple Schechter fit from Li & White (2009). We show the $\pm 1\sigma$ error on the model prediction for the RV as the shaded magenta region model as an example [DC: still adjusting this to bring each model into better agreement]

2.3 Populating Simulations

We build mock galaxy catalogues using the models and simulation described in the previous sections. For the rank order SHAM models, RM and RV, we use the triple piece-wise Schechter function fit to the stellar mass function, ϕ_{SDSS} , from Li & White (2009, LW09 hereafter). This stellar mass function is based on a complete sample of galaxies from SDSS and assumes a universal Chabrier (2003) initial mass function (IMF). We integrate the stellar mass function to get the cumulative stellar mass function:

$$N(> M_*) = V \int_{M_*}^{\infty} \phi_{\text{SDSS}}(M'_*) dM'_* \quad (24)$$

where V is the volume of the simulation being populated. We then normalize by the total number of galaxies above the threshold, $N_{\text{lim}} = N(> 10^{9.5} h^{-2} M_\odot)$, to get $F(M_*) = N(> M_*)/N_{\text{lim}}$, the cumulative probability distribution of galaxies as a function of stellar mass. We then draw from this distribution N_{lim} times using the inverse transform sampling method. In this way, each sampling is a Monte Carlo (MC) realization of the stellar mass function in the simulation volume. (Sub-)haloes are then populated by matching rank orders between stellar mass and (sub-)halo mass such that the most massive (sub-)haloes receive the most massive galaxies.

288 $M_{\text{vir}} = (4/3)\pi R_{\text{vir}}^3 \bar{\rho}_h$. Additionally, sub-haloes in this cat-
289 alogue are distinct, self-bound structures whose centre is
290 found within the virial radius of a more massive host-halo.
291 For each (sub-)halo, the maximum circular velocity is de-
292 fined as: $V_{\text{max}} \equiv \text{Max}[GM(< r)/r]$, where $M(< r)$ is the
293 mass enclosed within a distance r of the (sub-)halo centre.

294 From this catalogue we construct our mocks primarily
295 using three values for each (sub-)halo: M_{peak} , V_{peak} , and
296 z_{acc} . M_{peak} is defined as the peak virial mass a (sub-)halo
297 achieves over its history. In our halo catalogues, we retain
298 all (sub-)haloes that obtained a peak mass greater than fifty
299 times the particle mass, m_p . z_{acc} is roughly the redshift a
300 sub-halo is first accreted. V_{peak} is the peak value of the max-
301 imum circular velocity, V_{max} , a (sub-)halo obtains over the
302 course of its history. A detailed description of how each of
303 these quantities is calculated can be found in Appendix A.

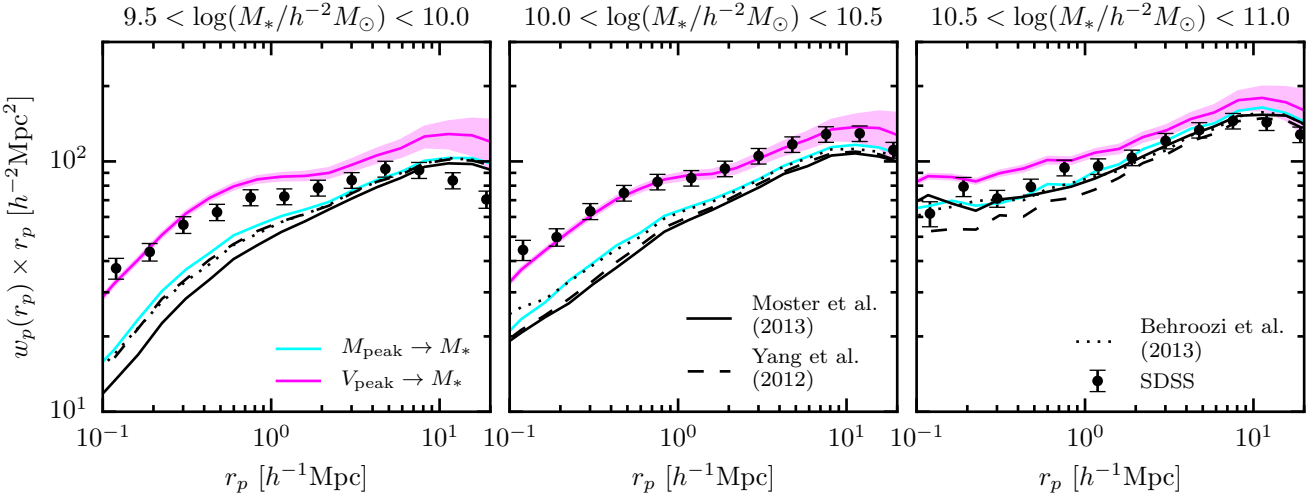


Figure 3. The projected correlation function, w_p , is plotted in three stellar mass bins for five SHAM models (lines). As an example, we show the $\pm 1\sigma$ error on the model prediction for the RV model as the shaded magenta region. For comparison, we plot the projected correlation function of galaxies in SDSS as measured by Yang et al. (2012) as points with error bars.

The parametrized SMHM models are populated in a different manner. The population of the simulation is a MC realization which begins by calculating the median stellar mass for each (sub-)halo and adding random scatter:

$$\log[M_*(M_{\text{peak}}, a_{\text{acc}})] = \log[\langle M_* | M_{\text{peak}} \rangle(a_{\text{acc}})] + \mathcal{N}(0, \sigma_{\log(M_*)}) \quad (25)$$

where $\mathcal{N}(0, \sigma_{\log(M_*)})$ is a random variable drawn from a normal distribution with mean 0 and a fixed log-scatter given by $\sigma_{\log(M_*)}$. We use $M = M_{\text{peak}}$ for all the models, but we confirm that using M_{acc} instead does not significantly affect our results.

This step is slightly complicated by the fact that each model's parameters were tuned using different halo mass definitions, $M_{\Delta_{\text{halo}}}$. The M13 model uses M_{200c} , Y12 uses M_{180m} , and B13 uses M_{360m} ⁵. As described in the previous section, our halo catalogue defines haloes as SO with masses given by M_{360m} . We use M_{peak} directly for the B13 model, and for the M13 and Y12 models we convert M_{peak} from M_{360m} masses to the appropriate version for each model using a fitting function, f_{conv} (see appendix C in Hu & Kravtsov 2003). In the conversion we assume all haloes are fit by an NFW profile (Navarro et al. 1997) and use halo concentrations measured by ROCKSTAR at the time M_{peak} is achieved, c_{peak} .

$$M'_{\text{peak}} = f_{\text{conv}}(M_{\text{peak}}, c_{\text{peak}}, \Delta_{\text{halo}}) \quad (26)$$

Furthermore, each of the evolving models was tuned using observations based on different methods of determining stellar mass. We apply a simple set of conversions in order to homogenize the stellar masses to a single system as described in Appendix B. We show the stellar mass function for a mock based on each model in Fig. 2. The stellar mass

⁵ The subscript “m” indicates the over-density with respect to the mean density of the Universe, while “c” is with respect to the critical density.

functions in each mock vary by up to ~ 0.2 dex from our fiducial stellar mass function used to create the RM and RV mocks. This is the result of each model being tuned with differing:

- (i) stellar mass functions, $\phi(M_*, z)$
- (ii) halo mass definitions/(sub-)halo finder
- (iii) cosmologies
- (iv) simulations which are subject to cosmic variance

While in principle each model could be re-fit using the same stellar mass function(s) and simulation, that is beyond the scope of this paper. We check that simple alterations to the parameters of each model which bring each into better agreement with the LW09 stellar mass function do not have a significant effect on the clustering signal predictions presented in §3. Given this, and the complexity involved in re-fitting each model, we use the parameters as they are quoted in each paper (and reproduced in table 2, with only minor alterations as discussed in the sections above).

3 CLUSTERING

In this section we present the galaxy clustering predictions of each SHAM model described in the previous section. We calculate the projected correlation function for each model, defined as:

$$w_p(r_p) = 2 \int_0^{r_{\parallel \text{max}}} \xi(r_{\parallel}, r_p) dr_{\parallel} \quad (27)$$

where r_{\parallel} is the separation parallel to the line-of-sight (LOS), r_p the separation perpendicular to the LOS, and ξ is the two-point correlation function. We set $r_{\parallel \text{max}} = 40 h^{-1} \text{Mpc}$ to mimic equivalent measurements made using SDSS galaxies (Yang et al. 2012). The choice of $r_{\parallel \text{max}}$ is a balance between minimizing the contribution of redshift space distortions to the measurement, and maximizing the signal to noise in

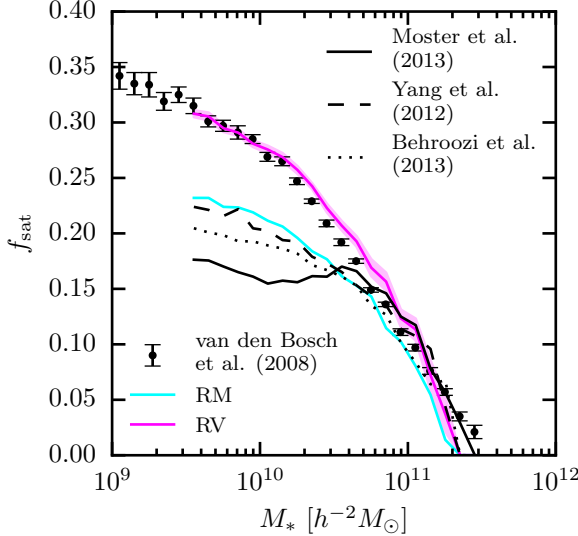


Figure 4. The satellite fraction as a function of stellar mass is plotted for SHAM model as lines. The models are RM (solid cyan), RV (solid magenta with the shaded region showing $\pm 1\sigma$ error on the model prediction), M13 (solid black), Y12 (dashed), and B13 (dotted). For comparison, we show the satellite fraction as inferred by van den Bosch et al. (2008) using a galaxy group catalogue of SDSS galaxies.

and observations is striking. Each halo mass-based models⁶ severely under-predicts the clustering signal in the two least massive bins (left two panels), while the RV model, based on V_{peak} , if anything, slightly over-predicts the signal. On the other hand, all the models considered here roughly predict an accurate clustering signal consistent with observations in the most massive stellar mass bin (right panel).

[add discussion of cosmic variance in the SDSS measurements]

The success of the RV model is consistent with findings by Reddick et al. (2013) who show that SHAM based on V_{peak} most closely matches galaxy clustering observations in SDSS, while all other halo properties under-predict the signal. We confirm that result here; furthermore, we show that more complicated evolving SMHM models based on M_{peak} do not alleviate the problem. In fact, evolution seems to exacerbate the clustering decrement of M_{peak} -based SHAM as evidenced by the RM model producing the strongest clustering signal amongst the mass-based models. The remainder of this paper examines why these models fail to produce strong enough clustering, why the RV model (and similar models) succeeds, and possible solutions to “save” mass-based SHAM models (under the assumption these models are worth saving).

4 THE V_{PEAK} MIRACLE

In this section, we examine the origin of the success of V_{peak} based SHAM models. By comparing the differences in V_{peak} and M_{peak} based models, we identify the culprit(s) in the failure of the mass-based models to match observational clustering measurements. We conclude the section by pointing out some deficiencies in V_{peak} SHAM.

4.1 The Satellite Fraction

In the mass-based models the clustering signal is most severely under-predicted at small scales ($< 1 h^{-1}\text{Mpc}$). This is a strong indication that the culprit is satellite galaxies—or more precisely, a lack of satellite galaxies in the mass-based SHAM models. With this in mind, we examine the satellite fraction, f_{sat} , in each model in Fig. 4. The RV model results in the largest number of satellites, approaching $\sim 30\%$ at $10^{9.5} h^{-2} M_{\odot}$, relative to the other models which remain below $\sim 24\%$. Comparing the clustering signals in Fig. 3 with f_{sat} in Fig. 4 shows that there is a nearly one-to-one correspondence between the clustering strength on small scales and f_{sat} in each model. Furthermore, f_{sat} between the models does not diverge until approximately $5 \times 10^{10} h^{-2} M_{\odot}$, above which the models largely agree with the observed clustering signal. Considering this, it may be more appropriate to restate the under-prediction of galaxy clustering in these models as an under-production of satellite galaxies.

434

the measurement (Padmanabhan et al. 2007; van den Bosch et al. 2013).

435

436

437

438

439

440

441

442

443

444

445

446

447

448

449

450

451

452

453

454

455

456

457

458

459

460

461

462

463

464

465

466

467

468

469

470

471

472

473

474

475

476

477

478

479

480

481

482

483

484

485

486

487

488

489

490

491

492

493

494

495

496

497

498

499

500

501

502

503

504

505

506

507

508

509

510

511

512

513

514

515

516

517

518

519

520

521

522

523

524

525

526

527

528

529

530

531

532

533

534

535

536

537

538

539

540

541

542

543

544

545

546

547

548

549

550

551

552

553

554

555

556

557

558

559

560

561

562

563

564

565

566

567

568

569

570

571

572

573

574

575

576

577

578

579

580

581

582

583

584

585

586

587

588

589

590

591

592

593

594

595

596

597

598

599

600

601

602

603

604

605

606

607

608

609

610

611

612

613

614

615

616

617

618

619

620

621

622

623

624

625

626

627

628

629

630

631

632

633

634

635

636

637

638

639

640

641

642

643

644

645

646

647

648

649

650

651

652

653

654

655

656

657

658

659

660

661

662

663

664

665

666

667

668

669

670

671

672

673

674

675

676

677

678

679

680

681

682

683

684

685

686

687

688

689

690

691

692

693

694

695

696

697

698

699

700

701

702

703

704

705

706

707

708

709

710

711

712

713

714

715

716

717

718

719

720

721

722

723

724

725

726

727

728

729

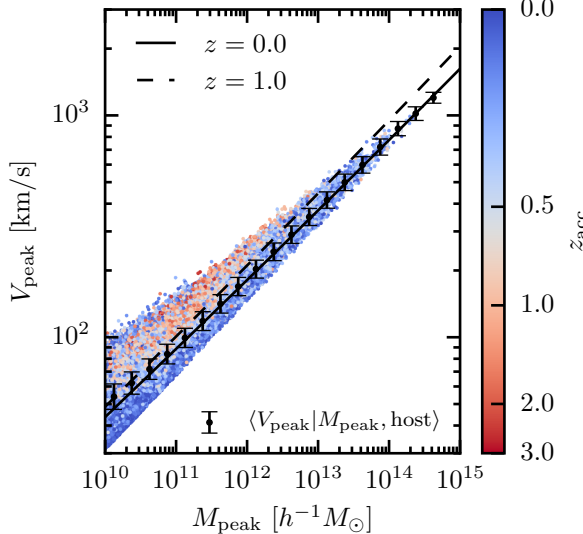


Figure 5. The relation between M_{peak} and V_{peak} is plotted for all sub-haloes in the Bolshoi simulation at $z=0$, colour-coded according to the redshift at the time of accretion, z_{acc} . For host-haloes, the median V_{peak} in 0.25 dex bins of M_{peak} is plotted as black points with error bars indicating the log-normal scatter. The solid line shows the median V_{peak} relation in eq. 32 at $z=0$. The dashed line shows the same relation at $z=1$. Sub-haloes have systematically higher values of V_{peak} than host-haloes at fixed M_{peak} .

4.2 Why is f_{sat} larger in V_{peak} SHAM?

As can be seen in Fig. 5, V_{peak} and M_{peak} are highly correlated properties of haloes with small scatter, $\sigma_{\log(V_{\text{peak}})} \sim 0.05$, at fixed M_{peak} for host-haloes. Additionally, sub-haloes have larger V_{peak} on average than host-haloes of equal M_{peak} . This difference between host-haloes and sub-haloes is a result of the correlation between halo formation history and concentration.

Assuming an NFW profile, V_{max} is an increasing function of the halo mass and concentration, c :

$$V_{\text{max}} = 0.465 V_{\text{vir}} \sqrt{\frac{c}{f(c)}} \quad (29)$$

where,

$$\begin{aligned} V_{\text{vir}} = & 159.43 \text{ km/s} \left(\frac{M_{\text{vir}}}{10^{12} h^{-1} M_{\odot}} \right)^{1/3} \left[\frac{H(z)}{H_0} \right]^{1/3} \\ & \times \left[\frac{\Delta_{\text{vir}}(z)}{178 \Omega_m^{-1}} \right]^{1/6} \end{aligned} \quad (30)$$

and,

$$f(x) = \ln(1+x) - \frac{x}{1+x} \quad (31)$$

Furthermore, it is a robust prediction of simulations of

⁶ As a short-hand, we will frequently refer to the RM, M13, B13, and Y12 models as ‘‘mass-based models’’.

ΛCDM structure formation that halo concentration correlates with halo formation time, $\langle z_f \rangle = g(M_{\text{vir}}, c)$ (e.g. Wechsler et al. 2002). Finally, because M_{peak} occurs before accretion for sub-haloes and near $z=0$ for host-haloes, sub-haloes generally have earlier formation times at fixed M_{peak} .

Using the concentration-mass-redshift relation from Macciò et al. (2009). We formulate a description for the median $M_{\text{peak}} - V_{\text{peak}}$ relation given by:

$$\langle V_{\text{peak}} | M_{\text{peak}} \rangle_{\text{med}}(z) = 1.1 \times \langle V_{\text{max}} | M_{\text{peak}} \rangle_{\text{med}}(z) \quad (32)$$

The factor of 1.1 accounts for the fact that the average peak maximum circular velocity is $\sim 10\%$ higher than V_{max} (Behroozi et al. 2014b). We show this relation at $z=0$ (solid line) and at $z=1.0$ (dashed line) in Fig. 5. At fixed M_{peak} , $\langle V_{\text{peak}} \rangle_{\text{med}}$ is larger at higher redshifts.

It is the correlated scatter in V_{peak} at fixed M_{peak} at $z=0$ which is responsible for the difference in satellite fractions between the RV and RM models. By populating (sub-)haloes by their rank on V_{peak} , more sub-haloes will be populated than would have been had M_{peak} instead been utilized for any given stellar mass threshold. This same reasoning carries over to the other mass-based models.

4.3 The Evolving Relation between M_{\star} and M_{halo}

Here we compare the RV model to the other models by examining the relation between stellar mass and halo mass that arises in each model, in the RV model by correlation between V_{peak} and M_{peak} , and in the other models by design. In the top panel of Fig. 6, we examine the relation between M_{\star} and M_{peak} in the RV model. The median stellar mass mass of central galaxies is shown as points with error bars indicating the log-normal scatter at fixed halo mass. The colour-coded points show the stellar mass of satellites. Beyond the ubiquitous broken power-law shape of the SMHM relation, sub-haloes ($z_{\text{acc}} > 0$) host more massive galaxies than host-haloes of equivalent M_{peak} , with earlier accreted satellites having the largest masses. This is precisely the expectation for satellites given the correlation between V_{peak} and formation time shown in the previous section.

We show the SMHM relation for the M13, B13, and Y12 models in the lower panels of Fig. 6; however, instead of showing individual satellite galaxies, we show the median relation as a function z_{acc} for simplicity and ease of interpretation. To the degree that satellites follow a different relation than centrals, the mass-based models predict the qualitative opposite trend as the RV model; sub-haloes host less massive galaxies than host-haloes of equivalent M_{peak} (at least for haloes less massive than $\sim 10^{12.5} h^{-1} M_{\odot}$). In the M13 and B13 models, this comes about because the SMHM relation for satellites as a function of z_{acc} serves as a fossil record of the SMHM relation for centrals at higher redshift, and Moster et al. (2013) and Behroozi et al. (2013c) find that the SMHM relation must evolve such that M_{\star} at fixed M_{peak} increases. This holds because it is assumed that satellites cease to grow after being accreted.

On the other hand, in the Y12 model there is no difference in $\langle M_{\star} \rangle_{\text{med}}$ between satellites and centrals at fixed M_{peak} . The Y12 model is different from M13 and B13 in that satellites are allowed to grow (or lose stellar mass) after z_{acc} . Yang et al. (2012) find that in the Y12 model

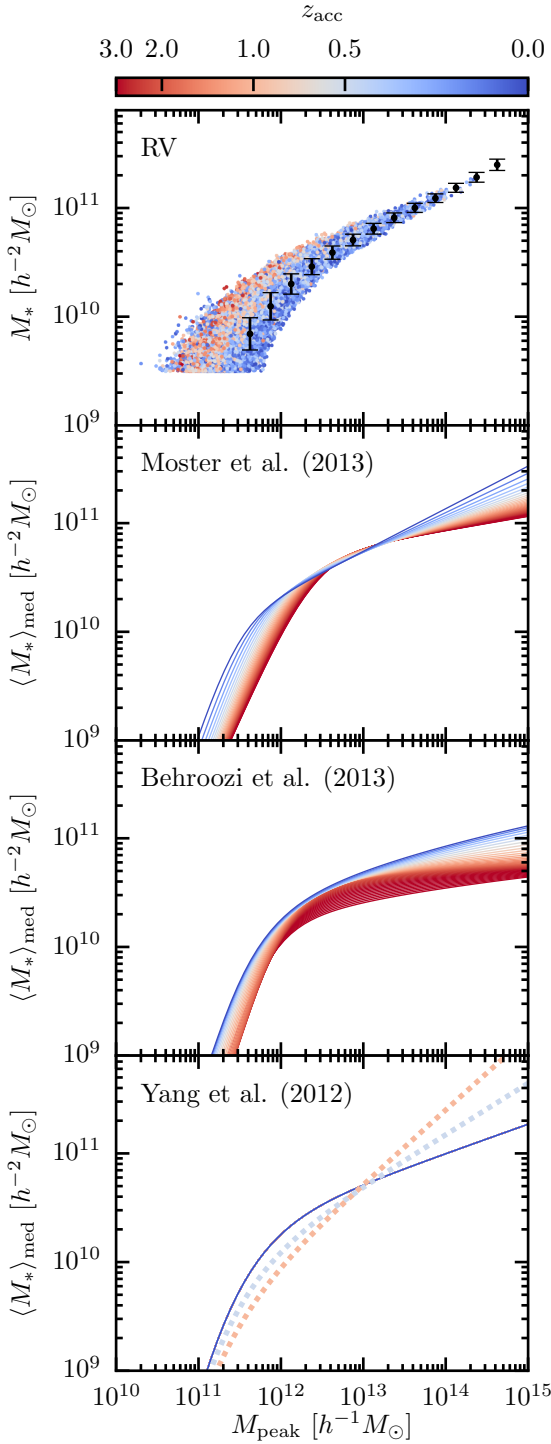


Figure 6. The SMHM relation in the RV model and the three evolving SHAM models. From top to bottom, the panels show RV, M13, B13, and Y12. For each model, the SMHM relation is shown at $z=0$ as a function of the redshift of accretion, z_{acc} , for satellites. The top panel shows the median stellar mass and scatter of central galaxies as points with error bars with satellites shown as colour-coded points. For the remaining panels, the analytic functions are shown. For these models, the relation for centrals is shown with z_{acc} set to 0. The dotted lines in the bottom panel give the relation for central galaxies at $z = 1$ and $z = 0.5$ as an example of the relation satellites that accreted at that time would follow if there were no evolution after accretion in the Y12 model.

529 post-accretion accretion evolution happens very efficiently—
 530 satellites achieve a final stellar mass $> 90\%$ that of centrals
 531 by $z = 0$. For simplicity, in this paper we have assumed that
 532 satellites obtain the same stellar mass as centrals (c parame-
 533 ter set to 1.0 in Y12), consistent with the uncertainty found
 534 by Yang et al. (2012). Therefore, all of the lines fall on top
 535 of each other in the bottom panel of Fig. 6. We also show
 536 the SMHM relation for centrals at $z = 0.5$ and 1.0 in the
 537 Y12 model as a dotted lines for comparison, and the relation
 538 satellites would follow with c set to 0.

539 This model for satellite growth is why the Y12 model
 540 predicts a slightly larger f_{sat} than the M13 and B13 models
 541 as shown in Fig 4. Because the sub-halo fraction increases
 542 as M_{peak} decreases (see §5 and Fig. 10), any model which
 543 boosts M_* in sub-haloes, will result in a larger fraction of
 544 satellites for any given stellar mass threshold. The same rea-
 545 soning holds for the RM model, relative to M13 and B13,
 546 where centrals and satellites always follow the same SMHM
 547 relation. However, this effect in the Y12 and RM models
 548 alleviates the clustering signal decrement only slightly com-
 549 pared to M13 and B13. In the absence of post-accretion evo-
 550 lution in M_* of satellites in Y12 (c parameter set to 0), the
 551 Y12 model appears similar to the M13 and B13 models
 552 where satellites are less massive than centrals at $z=0.0$ (be-
 553 low $\sim 10^{12.5} h^{-1} M_\odot$). It is interesting that in the analysis
 554 performed in Yang et al. (2012), they find $c \sim 1$ is strongly
 555 preferred over $c \sim 0$. We examine post-accretion evolution
 556 of satellites in more detail in §6.

4.4 Galaxy Growth Histories

558 Given that the RV and mass-based models make different as-
 559 sumptions for the SMHM relation, especially regarding satel-
 560 lites, it is not surprising that each model predicts different
 561 galaxy clustering signals and satellite abundances. Consider-
 562 ing the RV model’s success in fitting clustering observa-
 563 tions and the mass-based models failure (see §3), it appears
 564 that the RV model should be favoured as the more physical.
 565 However, in this section we show that the RV model implies
 566 galaxy growth histories that are incompatible with both the
 567 other models and observations.

568 In the previous section we showed that, in the RV
 569 model, the stellar masses of satellites are on average larger
 570 than centrals at fixed M_{peak} . This finding implies that the
 571 SMHM relation in the RV model evolves in the opposite di-
 572 rection as the mass-based models. This conclusion rests on
 573 two implicit assumptions of the RV model: the stellar mass
 574 of satellites does not evolve significantly after z_{acc} , and the
 575 $M_* - V_{\text{peak}}$ (SMVP) relation itself does not evolve. A non-
 576 evolving SMVP implies that galaxies grow along the SMVP,
 577 i.e. galaxy growth is tied to the growth of V_{peak} . In this
 578 section we examine the latter assumption, and we leave an
 579 examination of post-accretion satellite evolution to §6.

580 In order to extrapolate the SMVP relation in the RV
 581 model to less massive haloes, we fit it with a function of the
 582 form:

$$\langle M_* | V_{\text{peak}} \rangle_{\text{med}} = 2M_0 \left(\frac{V_{\text{peak}}}{V_0} \right) \left[\left(\frac{V_{\text{peak}}}{V_0} \right)^\alpha + \left(\frac{V_{\text{peak}}}{V_0} \right)^\beta \right]^{-1} \quad (33)$$

583 We perform a non-linear least squares fit to the median

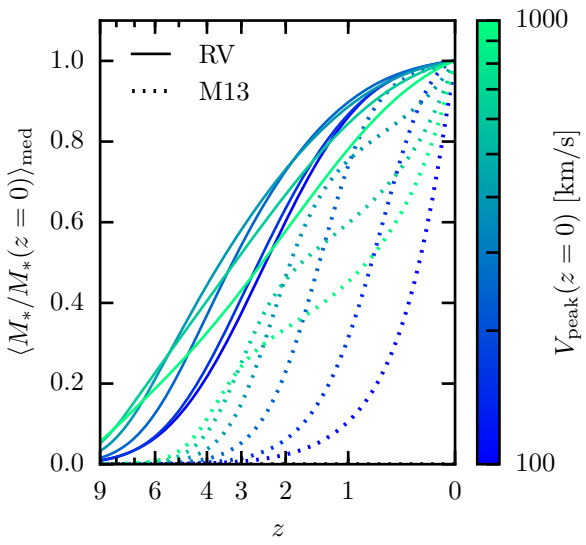


Figure 7. The average stellar mass as a function of redshift divided by the mass at $z=0$ for haloes of various values of V_{peak} at $z=0$ (coloured lines). The prediction from the non-evolving RV model is shown as solid lines. The prediction of the evolving M13 model is shown as dotted lines. $V_{\text{peak}}(z=0)$ was converted to M_{vir} using a fitting function in order to directly compare the RV and M13 models. The implied average stellar mass growth histories of haloes are drastically different between the two models. The RV model predicts much earlier stellar mass growth relative to the M13 model.

584 stellar mass in 0.025 dex V_{peak} bins. We find an excellent
 585 fit is provided by: $\log(M_0/h^{-2}M_\odot) = 10.0 \pm 0.01$,
 586 $\log(V_0/\text{km s}^{-1}) = 2.197 \pm 0.004$, $\alpha = -4.6 \pm 0.1$, and
 587 $\beta = -0.20 \pm 0.01$. We perform a similar fit to the SMHM
 588 relation in the RM model.

589 In addition to the form of the SMVP relation, the
 590 average growth history of galaxies in RV is dependent
 591 on the potential well growth history (PWGH) of haloes,
 592 $\langle V_{\text{peak}} | V_{\text{peak}}(z=0) \rangle_{\text{med}}(z)$. Using the PWGHs from van den
 593 Bosch et al. (2014), in Fig. 7 we show the implied growth
 594 history of galaxies in the RV model for host-haloes with dif-
 595 ferent V_{peak} at $z=0$. For comparison, we also show stellar
 596 mass growth histories from M13, which instead depend on
 597 the average mass accretion histories (MAHs) of haloes and
 598 the explicitly parametrized evolution of the SMHM relation.
 599 Note that we have converted $M_{\text{peak}}(z=0)$ to $V_{\text{peak}}(z=0)$
 600 using eq. 32 to place these histories on the same figure.

601 Fig. 7 shows that, in the RV model, galaxy growth
 602 is largely self-similar—at any given redshift, galaxies of ev-
 603 ery mass are growing at similar rates. Conversely, in the
 604 M13 model, galaxy growth is much more dependent on halo
 605 mass—high mass galaxies form early, growing slowly at low
 606 redshift, while low mass galaxies form late. Slow late time
 607 growth of massive galaxies is necessary to reproduce the ob-
 608 served prevalence of quiescent galaxies as mass increases
 609 (e.g. van den Bosch et al. 2008; Wetzel et al. 2012). This
 610 is related to the downsizing phenomenon (Neistein et al.
 611 2006), wherein star-formaiton shifts to less massive galax-

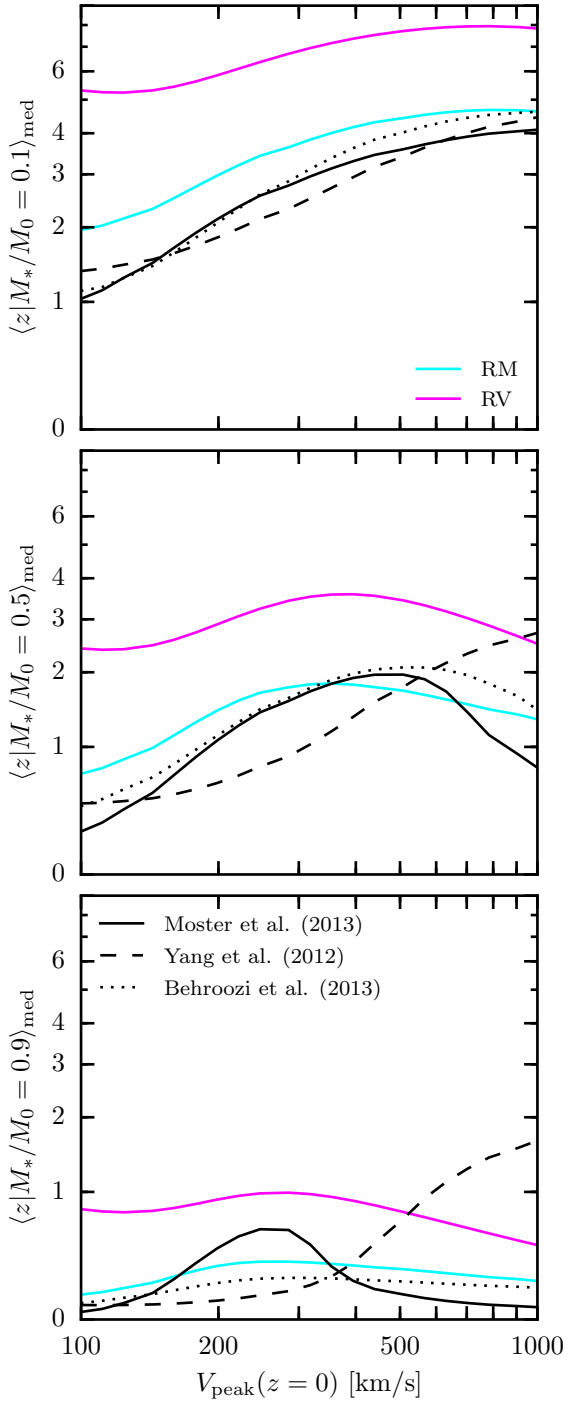


Figure 8. The median redshift at which a central galaxy reaches a fraction, f , of its $z=0$ stellar mass as a function V_{peak} at $z=0$. The three panels are for $f = 0.1, 0.5$, and 0.9 from top to bottom, respectively. The lines are for the RM (solid cyan), RV (solid magenta), M13 (solid black), Y12 (dashed), and B13 (dotted). The RV model consistently forms a larger fraction of galaxies' mass at higher redshift relative to the mass-based models.

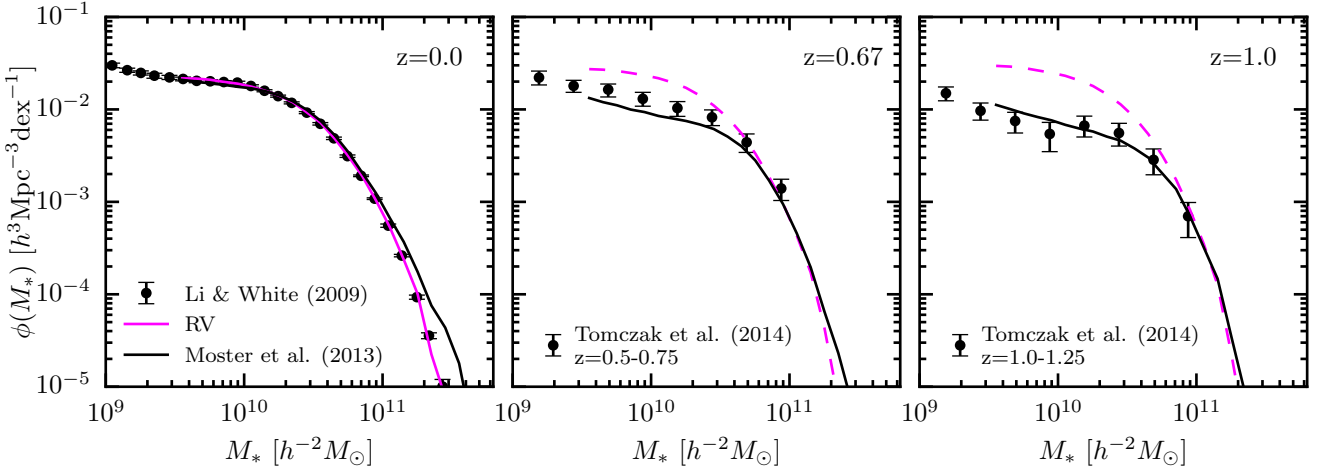


Figure 9. The evolution of the stellar mass function is shown for the M13 model (black lines) as well as the implied evolution of the RV model (magenta lines). For comparison, we show observational measurements of the stellar mass function from Li & White (2009) ($z=0$), and Tomczak et al. (2014) ($z>0$).

ies at low redshifts (e.g. Kodama et al. 2004; Jimenez et al. 2005; Juneau et al. 2005; Bell et al. 2005; Bundy et al. 2006).

It is the same story when comparing RV to any of the other mass based models. In Fig. 8, we show the median redshift galaxies formed a fraction, f , of their $z=0$ stellar mass (this is another way of examining the information in Fig. 7). The top panel shows median redshift galaxies formed 10% of their mass. The middle and bottom panels show the redshift for 50% and 90% respectively. The primary conclusion to draw from this is that the mass-based SHAM models generically predict much later growth compared to RV. Interestingly, even the RM model, where the SMHM relation does not evolve, results in galaxy growth much closer to the evolving models than with RV. This is a consequence of the fact that haloes form their potential wells early, primarily adding mass in the outskirts at late times (van den Bosch et al. 2014). As a result, any model for galaxy formation based on V_{peak} will have to decouple galaxy growth from the growth of V_{peak} more than models based on M_{peak} .

Finally, the effect of the dramatically different growth history in the RV model can be seen in the evolution of the stellar mass function. In Fig. 9 we show the predicted stellar mass function, $\phi(M_*, z)$, in the RV model and M13 (which was tuned to reproduce $\phi(M_*, z)$). Here it is clear that the RV model over-produces galaxies at high redshift, especially below the knee in the mass function.

SMVP relation. Any evolution will require the SMVP relation to be lower at high redshifts (as is the case for the SMHM relation in M13, Y12, and B13), reducing the stellar mass assigned to satellite galaxies in typical implementations. This sort of modification would result in a decrease in the galaxy clustering signal on small scales. We leave formulations of evolving V_{peak} to future work.

Given this failure of the V_{peak} SHAM, it is not clear that there is a reason to prefer a V_{peak} based SHAM model over models based on M_{peak} . Furthermore, apart from arguments related to fitting $w_p(r_p)$ and $\phi(M_*, z)$, there are other difficulties that must be overcome if V_{peak} is to be argued as more fundamental in driving the stellar mass mapping into (sub-)haloes. For any given (sub-)halo, V_{peak} is generally set during major mergers (1:5 or larger, Behroozi et al. 2014a), and if stellar mass is tightly correlated with V_{peak} , this could imply bursty star-formation closely tied to major mergers which is not favoured by observations (e.g. star formation histories, Diemer et al. 2017). On the other-hand, M_{peak} remains a theoretically attractive quantity that should be tightly coupled to stellar mass. Peak halo mass should be a good indicator of the amount of gas that has been accreted and thus in principle available to a galaxy to form stars over its history. Nevertheless, it is possible that feedback processes that result in the modulation of star-formation efficiency happen to correlate with V_{peak} , but this remains unclear.

In our comparison between V_{peak} -based SHAM and M_{peak} -based SHAM it is clear that there is a tension between fitting galaxy clustering on small scales while simultaneously reproducing the build up of stellar mass in the Universe. This tension presents a “clustering crisis” for SHAM. Our exploration of the reasons for this tension suggests multiple ways SHAM models could be altered in order to alleviate this crisis. We have identified too few satellites as the primary culprit for the clustering deficiency in mass based SHAM models. One avenue to address this problem is to simply in-

4.5 V_{peak} or M_{peak} ?

Given that the M13, Y12, and B13 models were fit to the stellar mass function at various redshifts and reproduce the cosmic star-formation density in the Universe (among other observables), it is difficult to imagine how to make a model like RV consistent with these same observational constraints. While not explored here, it is likely that a more complicated V_{peak} based SHAM model could produce realistic galaxy growth histories, but this would require evolution in the

crease the number of satellites in the mass-based models as many models have found to be necessary. In §5, we examine the plausibility of missing sub-haloes, and thus satellites, in our implementation of the mass-based SHAM models. A significant population of missing sub-haloes would be an indication that so called “orphan” galaxies play an important role in solving the clustering crisis. Apart from orphans, we also consider two other physically motivated modifications to increase the satellite fraction: post-accretion satellite growth in §6 and assembly bias effects in §7.

5 ORPHAN GALAXIES

One possible solution to the lack of small scale clustering signal in SHAM models is to include a population of “orphan” galaxies. Given the finite mass and force resolution of dark matter simulations, it is reasonable to expect that some sub-haloes are artificially disrupted or otherwise missing from the halo catalogues at $z=0$ (Carlberg 1994; van Kampen 1995; Guo & White 2013, van den Bosch 2017 in prep.). Alternatively, sub-halo finders may fail in identifying sub-haloes when the density contrast is low (Wetzel & White 2010; Muldrew et al. 2011; Knebe et al. 2011; Onions et al. 2012; Knebe et al. 2013; van den Bosch & Jiang 2016) as is the case in the central regions of host haloes. If this is in fact occurring, then it is appropriate to include a population of “orphan” galaxies, galaxies that have no identifiable sub-halo within a simulation but should rightfully be included if the simulation or sub-halo finder had been more successful.

After sub-haloes are accreted onto a more massive host halo, mass is tidally stripped as the sub-halo orbits within the potential of its host, resulting in a ratio between the $z = 0$ mass and the mass at accretion that is generally less than unity:

$$f_m = m_{\text{sub}}/m_{\text{acc}} \quad (34)$$

where the mass of a sub-halo, m_{sub} , is the instantaneous mass that is bound to the sub-halo, and m_{acc} is the virial mass at the time of accretion. Eventually, sub-haloes may simply be stripped below the mass resolution of the simulation, $f_m \times m_{\text{acc}} \sim m_p$. If it is common for sub-haloes to survive to this point, this will result in a need for orphans. Alternatively, if sub-haloes are not tracked accurately, mass resolution is not sufficiently high, or the force resolution is not sufficient, some sub-haloes may become disrupted prematurely, meaning fewer sub-haloes will be available to host satellite galaxies when applying an abundance matching scheme.

Here we estimate the contribution of this potential missing sub-structure to the abundance of sub-haloes. In the upper panel of Fig. 10, we measure the sub-halo fraction as a function of M_{peak} at $z=0$ in 0.2 dex mass bins:

$$f_{\text{sub}} = \frac{N_{\text{sub}}}{N_{\text{sub}} + N_{\text{host}}} \quad (35)$$

Jiang & van den Bosch (2016) and van den Bosch & Jiang (2016) show that the evolved conditional sub-halo mass function is well approximated by a power law with a universal low mass end slope. Given this, it is expected that f_{sub} will be a monotonic power law, increasing towards lower halo masses.

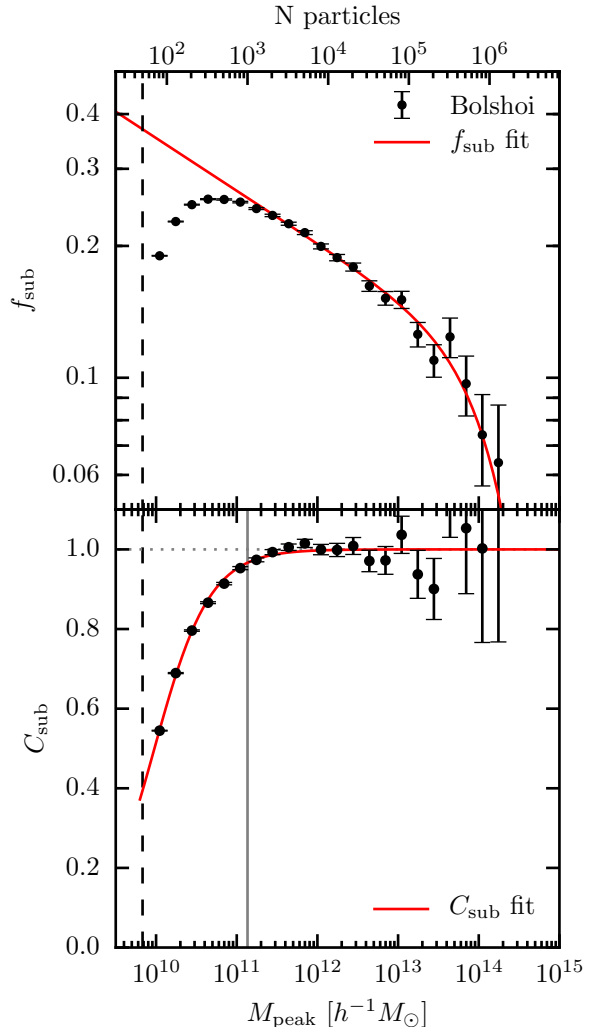


Figure 10. The upper panel shows the fraction of haloes that are sub-haloes, f_{sub} , as a function of M_{peak} in the Bolshoi simulation (points with error bars). This relation is fit with a Schechter function (eq. 36, red line) down to $10^{12} h^{-1} M_{\odot}$ and extrapolated to lower masses. The lower panel shows an estimate of the sub-halo completeness, C_{sub} . This relation is fit with a function (eq. 37, red line). The dashed line marks the 50 particle M_{peak} minimum mass a (sub-)halo must attain to be included in our halo catalogue. The grey line indicates the 1000 particle mass limit Guo & White (2013) recommend for convergence in sub-halo abundance. The upper x-axis is the number of particles corresponding to M_{peak} on the lower axis. The error bars indicate Poisson Errors.

With this in mind, we fit f_{sub} in Bolshoi with a Schechter function of the form:

$$f_{\text{sub}}(M_{\text{peak}}) = f_0 \left(\frac{M_{\text{peak}}}{M_0} \right)^{\alpha} e^{-M_{\text{peak}}/M_0} \quad (36)$$

We find a good fit with $f_0 = 0.105 \pm 0.006$, $\log(M_0/h^{-1} M_{\odot}) = 13.4 \pm 0.1$, and $\alpha = -0.120 \pm 0.005$ as shown as the red line in the upper panel of Fig. 10. There is a prominent break in the the sub-halo fraction at $\sim 10^{11} h^{-1} M_{\odot}$, approximately 1.5 dex above the halo

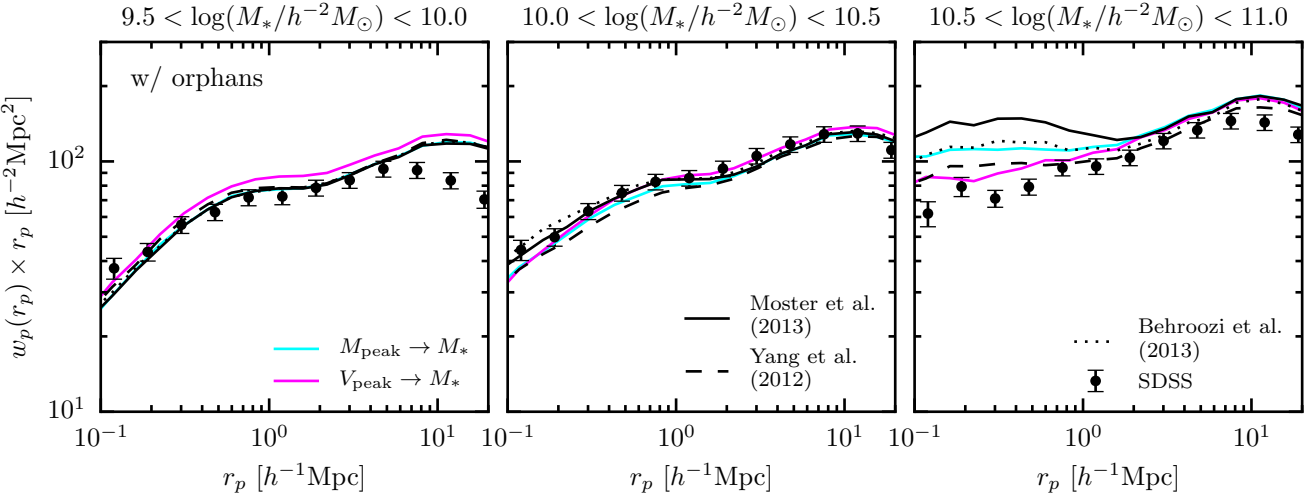


Figure 11. The projected correlation function, w_p , is plotted in three stellar mass bins for five SHAM models (lines) where we have introduced orphan galaxies into each model in order to approximately match the clustering in the [10.0,10.5] log stellar mass bin. For comparison, we plot the projected correlation function of galaxies in SDSS as measured by Yang et al. (2012) as points with error bars. Compare this to figure 3 for the case with no orphans.

mass identification limit imposed on the simulation, $50 \times m_p$. Therefore, we conservatively use only the measurements above $10^{12} h^{-1} M_\odot$ for our fit to f_{sub} .

We calculate the sub-halo completeness in the simulation as the ratio of the empirical f_{sub} and the fit using eq. 36 as shown in the bottom panel of Fig. 10. We then model the completeness, C_{sub} , as a function of halo mass as:

$$C_{\text{sub}}(M_{\text{peak}}) = \frac{C_0}{1.0 + \left(\frac{M_0}{M_{\text{peak}}}\right)^\gamma} \quad (37)$$

We find $\log(M_0/h^{-1} M_\odot) = 9.980 \pm 0.003$ and $\gamma = 1.27 \pm 0.02$ provides a good fit, as shown by the red line in the bottom panel in Fig. 10. For now, we fix $C_0 = 1.0$, and we examine the possibility of $C_0 < 1.0$ at the end of this section. The implicit assumption here is that when sub-haloes are well resolved, as is the case for massive (sub-haloes) at the time of infall, there should be no missing sub-structure. Our estimation of the completeness is broadly consistent with the 1000 particle threshold found by Guo & White (2013) using the Millennium simulation suite (shown as the grey line in the bottom panel of Fig. 10). Furthermore, we find that $C_{\text{sub}}(M_{\text{peak}})$ is very nearly constant with redshift (between $z = 0 - 4$).

The SHAM models considered in this work require sub-haloes in order to populate the simulation with satellites. To create sub-haloes to host orphan galaxies we “clone” extant sub-haloes in the regime where incompleteness results in too few sub-haloes. Here we briefly describe this process, and we provide a more detailed description in Appendix C. Where needed, we create a copy of a sub-halo (hereafter ‘clone’) and place it into a new host-halo with approximately the same mass as the donor’s host-halo. We consider two methods for assigning positions and velocities to these new clone sub-haloes that host orphans. One method conserves the relative position and velocity with respect to the donor’s host-halo (**sub-profile**). The other method assigns the clone the posi-

tion and velocity of a randomly selected dark matter particle in its new host-halo (**dm-profile**). We carry over all other relevant properties from donor to clone (e.g. z_{acc}). We then add clones into the simulation to make up for incompleteness.

We find that when populating the Bolshoi simulation down to $M_* \geq 10^{9.5} h^{-2} M_\odot$ using our model for C_{sub} , less than $\sim 1\%$ of satellite galaxies are orphans in each of the SHAM models. This small orphan percentage suggests that the Bolshoi simulation has sufficient resolution for SHAM studies down to the stellar masses considered in this paper. Of course, populating these models down to lower masses would result in a larger contribution from orphans. Nevertheless, we examine the effect of this small orphan population on the galaxy clustering predictions of each SHAM model. While not shown here, we find that the maximum effect on w_p is of order $\sim 1\%$ on the clustering signal at $0.1 h^{-1} \text{Mpc}$, regardless of the method used to assign orphan positions in their host. As expected, the effect of these orphans is even smaller in the more massive stellar mass bins were the C_{sub} correction is smaller. We conclude that the resolution of the Bolshoi simulation appears to be sufficient for SHAM studies down to the stellar masses considered here and most relevant for galaxy clustering studies using SDSS.

Finally, we ask “how many orphans are needed to increase the clustering signal sufficiently in the SHAM models based on M_{peak} to match observations?” To answer this question, we adjust C_0 in eq. (37), while keeping the other parameters fixed, and fit to the galaxy clustering observations. Lower values of C_0 imply an overall increased population of clone sub-haloes available to host orphans at all masses. This correction assumes that sub-haloes are being artificially disrupted or merged with the host *at all masses*. For each model, C_0 was adjusted in order to best fit the galaxy clustering signal in the intermediate mass bin ($10.0 \leq \log(M_*/h^{-2} M_\odot) < 10.5$). The result of this exer-

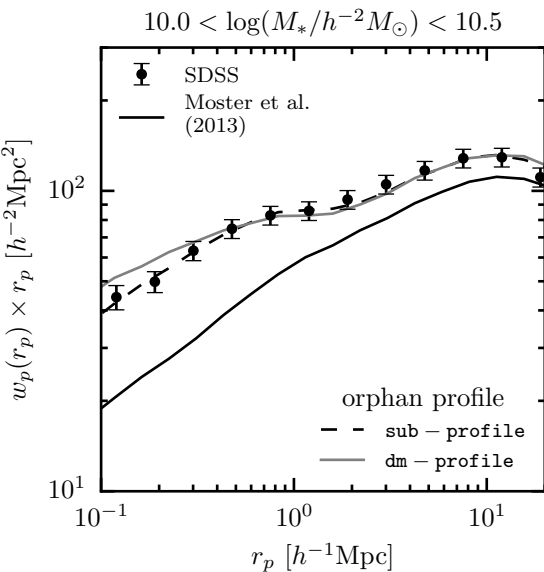


Figure 12. Comparison of the effect of the profile orphan galaxies follow in their host-halo on galaxy clustering. The solid line shows the clustering prediction for the original M13 model. The dashed line is M13 including orphans which follow the same profile as extant sub-haloes in the simulation with $C_0 = 0.4$. The grey line is the same model where orphans are more centrally concentrated, following the profile of dark matter in their host. See Appendix C for a more detailed discussion. For comparison, SDSS measurements by Yang et al. (2012) are plotted as points with error bars.

cise is shown in Fig. 11 using the **sub-profile** method to assign the positions and velocities. We find that each model requires $C_0 = [0.6, 1.0, 0.4, 0.5, 0.5]$, for the RM, RV, M13, Y12, and B13 models respectively. While the RV model does not require orphans, the mass-based SHAM models require that on average approximately *half of all satellites are orphans*.

In Fig. 12 we show how assigning orphans' positions within their host affect the clustering predictions for the M13 model in the intermediate mass bin only. As expected, using **dm-profile** boosts the clustering signal at small scales relative to **sub-profile**, but the effect is small compared to the dependence on C_0 . This trend is largely similar in the other mass bins considered and for the other SHAM models. The exact profile followed by orphans is a secondary effect compared to the large abundances required.

We make no attempt to fit for new parameters in the evolving SMHM models using our orphan model and clustering measurements, while the RM and RV models adjust automatically to the increased abundance of sub-haloes. Adjusting the population of sub-haloes so drastically in the evolving models will have an effect on the parameter inference for the SMHM relation. the stellar mass function in these models changes by $\sim 10\%$. With this caveat in mind, the most noticeable failure of the mass-based models is the over-prediction of the small scale ($< 1 \text{Mpc}$) clustering signal in the most massive stellar mass bin ($10.5 \leq \log(M_*/h^{-2} M_\odot) < 11.0$). Each of these models now produce

too many massive satellites. This problem could be reduced by altering the SMHM for massive satellites or reducing the number of massive orphans. We leave a detailed study on the self-consistency of including orphan galaxies in SHAM to future work.

The Y12 model model when fit to galaxy clustering in Yang et al. (2012), which used an analytic halo model and let the sub-halo abundance be a free parameter, finds results which are consistent with our finding here that $C_0 \sim 0.5$, namely that the sub-halo abundance needs to be approximately a factor of two larger than in the Bolshoi simulation. Furthermore, Jiang & van den Bosch (2016) find that the un-evolved (peak sub-halo mass) surviving (not disrupted) sub-halo mass function is approximately a factor of two lower than the un-evolved sub-halo mass function. This suggest a plausible source of the missing sub-haloes needed to host orphans could be artificially disrupted sub-haloes.

6 SATELLITE GROWTH

While we have shown that a large population of orphan galaxies could alleviate the clustering crisis in mass-based SHAM models, high resolution dark matter simulations do not seem to provide evidence of the requisite missing sub-halo population. With this in mind, we explore alternative mechanisms to boost the galaxy clustering signal in SHAM models. In this section, we consider whether continued star-formation in satellites after accretion can significantly boost clustering. This is motivated by findings that suggest satellites continue to form stars and grow in stellar mass after accretion for between ~ 2 and 4 Gyr (Wetzel et al. 2013). If satellites continue to grow after accretion, SHAM methods which use the SMHM relation at z_{acc} to assign stellar mass to satellites will under-estimate M_* in sub-haloes (e.g. M13 and B13).

It is a common assumption in SHAM models, implicit or explicit, that satellites undergo no significant evolution in stellar mass after z_{acc} . Amongst the models considered in this work, Y12 serves as an exception, explicitly parametrizing post-accretion evolution. In the bottom panel of Fig. 13, we provide a graphic in order to explain how growth is parametrized in Y12. Satellites (broken blue lines) are assigned a stellar mass at $z=0$ that is between the one achieved at z_{acc} and the one a central galaxy with equivalent M_{peak} at $z=0$ achieves (solid blue line). The growth (or mass loss) of satellites is controlled by the “ c ” parameter in eq. (22). In the case where $c=1$ (dotted blue line), satellites reach the same mass as corresponding central galaxies, and as a result satellites follow the same SMHM relation as centrals at $z=0$, regardless of z_{acc} . In the case where $c=0$ (dashed blue line), the Y12 model is similar to B13 and M13, where there is no evolution in the mass of satellites after z_{acc} . For this work, we set $c=1$ (consistent with SMF2 FIT-2PCF in table 4 in Yang et al. 2012). The result of setting $c=1$ is a model similar to the RM model, where no distinction is made between host-haloes and sub-haloes when abundance matching on M_{peak} at $z=0.0$. While such a model does produce more massive satellites than the M13 and B13 models, the RM and Y12 models still result in a clustering signal that is too weak on small scales.

In order to further explore the effect of satellite growth,

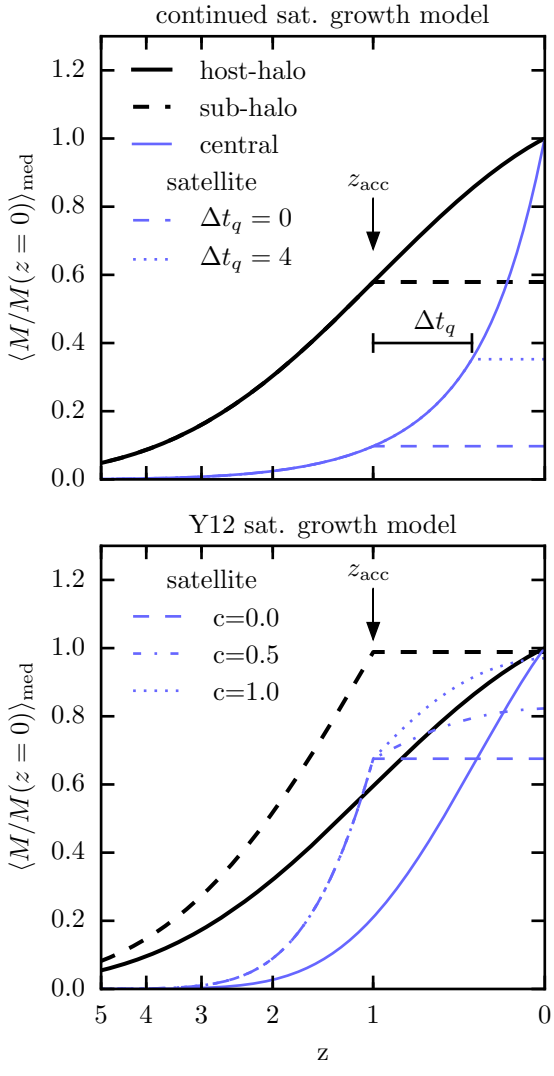


Figure 13. In this figure, we show two models for post-accretion satellite evolution used in this paper. In both panels, the median mass accretion history (MAH) of an example host-halo (solid black line) and sub-halo accreted at $z = 1$ (dashed black line) are shown. For the sub-halo, we show the peak mass. Top panel: continued satellite growth model described in §6. We show the median stellar mass of a central galaxy which occupies a halo with a $z=1$ mass of $10^{11} h^{-1} M_\odot$ in the M13 model (solid blue line). The median stellar mass of a satellite for different values of Δt_q is indicated by blue dashed and dotted lines for a sub-halo with the same mass at accretion onto an unrelated host-halo. In each case, the halo (galaxy) growth histories are normalized by the $z=0$ mass of the host-halo (central galaxy). Bottom panel: the satellite growth model in Y12 described in §2.1.4. Here, the sub-halo instead has the same mass at accretion as the host-halo at $z = 0$. The growth history of a satellite for different values of the c parameter is shown as various blue lines.

we devise a different model for post accretion evolution similar to that implemented in Behroozi et al. (2015). Our primary assumption is that satellites continue to form stars exactly like central galaxies which occupy haloes that had the same mass as the satellite's halo at the time of accretion, $t_{\text{acc}}(z_{\text{acc}})$, before quenching rapidly after a delay time, Δt_q . Within the SHAM framework, stellar mass is assigned to (sub-)haloes using a mass proxy, \mathcal{M} . To implement our growth model, we set \mathcal{M} for sub-haloes to the average mass of a host-halo at $t_{\text{acc}} + \Delta t_q$ which had the same mass as the sub-halo at t_{acc} :

$$\mathcal{M} = \langle M_{\text{vir}}(t_{\text{acc}} + \Delta t_q) | M_{\text{vir}}(t_{\text{acc}}) = M_{\text{acc}} \rangle_{\text{med}} \quad (38)$$

To extrapolate the mass from t_{acc} to $t_{\text{acc}} + \Delta t_q$ we again use the median MAHs from van den Bosch et al. (2014).

In the upper panel of Fig. 13 we describe the components of this ‘‘continued satellite growth’’ model. Consider two galaxies, one destined to be a central galaxy at $z=0$, and another that becomes a satellite at $z=1$. Each galaxy resides in a halo with mass $10^{11} h^{-1} M_\odot$ at $z=1$. We show the MAH for such a host-halo and sub-halo normalized by the $z=0$ mass of the host-halo as a black solid and dashed line in Fig 13. The stellar mass growth history for a central galaxy in such a host-halo in the M13 model is shown as a solid blue line, and the growth history of a satellite galaxy is shown as a long dashed blue line, each normalized by the stellar mass of the central at $z = 0$. In a model where no evolution occurs post-accretion, the stellar mass of the satellite is set at z_{acc} . An example of the continued growth model is shown as a dotted blue line—the satellite continues to grow for Δt_q after z_{acc} just as it would have had it remained a central. In this specific example, the satellite's stellar mass increases by 350% compared to M13 with no post-accretion growth when $\Delta t_q = 4 h^{-1}\text{Gyr}$. In general, the amount a satellite will grow in a fixed Δt_q depends on z_{acc} , M_{peak} , and the evolution of the SMHM relation. Recently accreted sub-haloes will have less time to grow, and massive sub-haloes will only grow slightly as massive galaxies do not grow rapidly at late times in most evolving models.

We apply this ‘‘continued satellite growth’’ model to the M13 and B13 models. Initially, we set $\Delta t_q = 4 h^{-1}\text{Gyr}$, the largest time found by Wetzel et al. (2013). As an example, we show the result on the clustering signal for the M13 model in Fig. 14 (purple dashed line). In each model, $\Delta t_q = 4 h^{-1}\text{Gyr}$ does not result in a sufficient increase in the clustering signal. To estimate an upper bound on the effect of such a satellite growth model, we allow satellites to grow till $z = 0$. This result is shown in Fig. 14 as a red dashed red line. Even this extreme satellite growth model does not result in strong enough galaxy clustering relative to observations. The results for the B13 model are very similar.

The failure of a continued growth model for satellites to fit galaxy clustering observations suggest that satellite growth (at least as implemented here) cannot on its own solve the clustering crisis; however, reasonable growth does have a significant effect on the clustering signal at small scales. This also suggests that the growth model used by Y12 is not sufficient to capture post-accretion growth. In Y12, a satellite is limited to grow only as massive as a central at $z=0$ with the same peak mass. In the growth model considered here, satellites may grow more massive than cen-

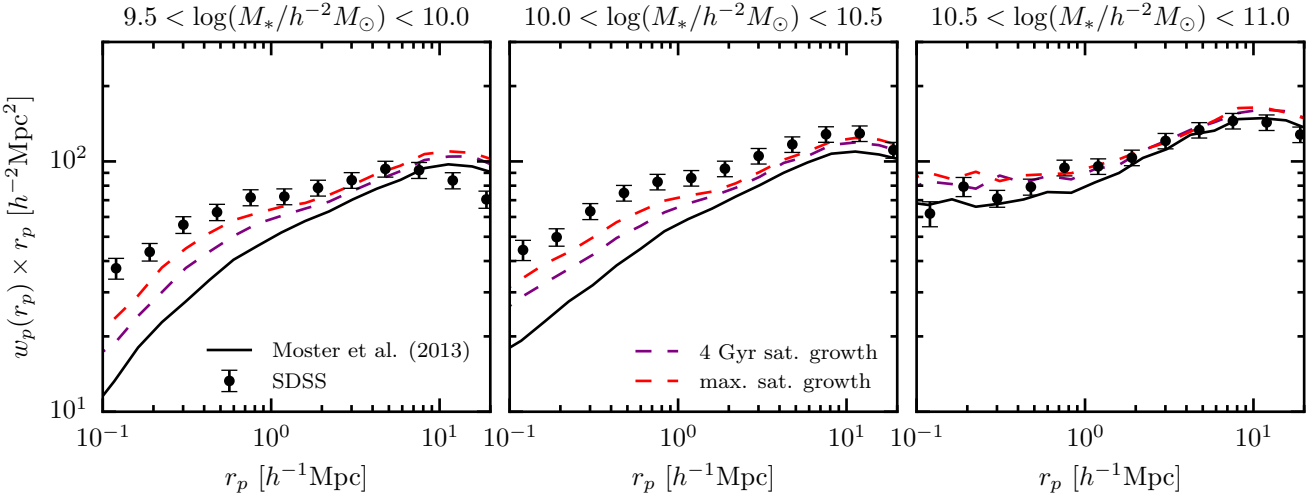


Figure 14. Similar to figure 3. The original M13 model is shown as a solid line. The effect of allowing satellites to grow as described in §6 for 4 Gyr (purple dashed line) and till $z=0.0$ (red dashed line).

trials by $z=0.0$. Any SHAM model that aims to fit galaxy clustering should take such an effect into account.

7 GALAXY ASSEMBLY BIAS

Assembly bias is a phenomenon observed in Λ CDM simulations of structure formation that the clustering of haloes depends on formation history in addition to mass (Gao et al. 2005; Wechsler et al. 2006; Gao & White 2007; Li et al. 2008; Sunayama et al. 2015). However, the degree to which the properties of galaxies themselves are influenced by the assembly history of their halo remains an open question, i.e. galaxy assembly bias. SHAM algorithms that employ measures of V_{\max} (like the RV model) already induce assembly bias into galaxies because concentration, and therefore circular velocity, is correlated with formation history at fixed halo mass (Zentner et al. 2014). Conditional abundance matching (CAM, Hearin et al. 2014) extends the SHAM framework by allowing for two or more halo properties to influence how galaxy properties are assigned in the SHAM algorithm. CAM has been used to study the dependence of star-formation rate and halo formation history (Hearin & Watson 2013; Hearin et al. 2014; Watson et al. 2015; Saito et al. 2015; Paranjape et al. 2015); however, SHAM models that assign stellar mass and star-formation in a self-consistent manner are still in development.

In this section we examine whether introducing assembly bias into the galaxy-halo mapping can increase the satellite fraction and galaxy clustering signal in mass-based SHAM models. Specifically, we consider a model where M_* is correlated with the formation history of the (sub-)halo it occupies such that early forming haloes host more massive galaxies than late forming haloes at *fixed* peak (sub-)halo mass. While many measures of halo formation history have been employed in the literature, for this work we use the redshift at which a halo first achieves a fraction, f , of its peak halo mass, z_f (see Appendix A for details on how z_f is calculated).

7.1 Rank Order SHAM Assembly Bias

We begin by modifying the RM model to include galaxy assembly bias. In order for assembly bias to have any effect on M_* , there must be a significant amount of scatter in the SMHM relation, $\sigma_{\log(M_*)} > 0$. Scatter provides a dynamic range in M_* at fixed M_{peak} over which M_* can be correlated with formation history. In Fig. 15, we show some constraints on $\sigma_{\log(M_*)}$ from the literature. Typical values found for $\sigma_{\log(M_*)}$ are between 0.1 – 0.2 dex (More et al. 2011; Reddick et al. 2013; Zu & Mandelbaum 2015b; Tinker et al. 2016); however, these values are most strongly constrained at high masses, $M_{\text{vir}} > 10^{12} h^{-1} M_\odot$. We add scatter to the SMHM in the RM model using the method from Behroozi et al. (2010), parametrizing the level of scatter as a function of halo mass, $\sigma_{\log(M_*)}(M_{\text{peak}})$.

To induce a correlation between M_* and z_f , we apply the CAM method by binning (sub-)haloes in small 0.1 dex M_{peak} bins. We then rank order (sub-)haloes by z_f and galaxies by M_* , re-assigning the most massive galaxies to the earliest forming (sub-)haloes in the bin. We use $f = 0.5$, the redshift where a (sub-)halo reaches half its peak mass. Furthermore, we parametrize the strength of this correlation by the Spearman's rank order correlation coefficient, $\rho(M_{\text{vir}})$. We are able to weaken the correlation by degrading the rank ordering as described in appendix D in order to reduce the effect of assembly bias on M_* . In this way, we can set the correlation strength as a function of stellar mass, $\rho(M_*)$.

Initially we try a model with fixed scatter, $\sigma_{\log(M_*)} = 0.18$ dex (similar to the other mass-based models), and a constant maximum correlation ($\rho = 1$) between M_* and z_f . This model produces a poor fit to the observed galaxy clustering signal. The satellite fraction of massive galaxies in such a model is unrealistically large. As a result, the clustering signal increases dramatically at high stellar masses, while at the same time, there is relatively little effect on the clustering signal at the lower stellar masses where the clustering is under-predicted. This can be understood as a result of the SMHM relation becoming steep at the low mass end,

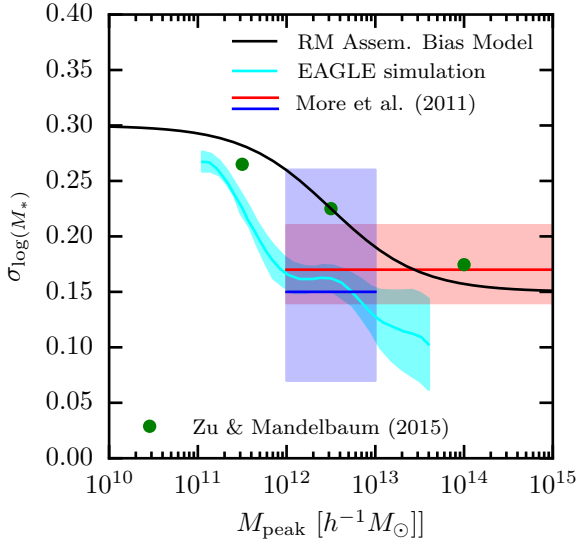


Figure 15. Here we plot the log-normal scatter in stellar mass as a function of peak halo mass for our model as a solid black line. For comparison, we show various measurements and theoretical prediction for the scatter. The cyan line and shaded region shows the relation for central galaxies in the EAGLE simulation with the 1-sigma errors (Matthee et al. 2016). The red and blue lines with shaded regions show the fixed scatter determined for red and blue central galaxies and the associated error measured from satellite kinematics (More et al. 2011). The green points show the scatter at three masses determined from an HOD analysis with weak lensing measurements (Zu & Mandelbaum 2015b).

and ~ 0.18 dex scatter in the SMHM relation is not sufficient to increase the satellite fraction significantly.

With this in mind, we modify our model to fit the observed galaxy clustering signal by modifying the parametrization of $\sigma_{\log(M_*)}$ and $\rho(M_{\text{vir}})$. First, we require the scatter to increase at lower halo masses ($< 10^{12} h^{-1} M_{\odot}$) and decrease at high halo masses ($> 10^{12} h^{-1} M_{\odot}$) where there are observational constraints. While there are few constraints on the scatter in low mass haloes, there are some indications that it may increase as mass decreases. In Fig. 15, we show some observational and theoretical constraints on $\sigma_{\log(M_*)}$.

We model the dependence of $\sigma_{\log(M_*)}$ on M_{peak} in the RM model as:

$$\sigma_{\log(M_*)}(M_{\text{peak}}) = f(M_{\text{peak}}) \quad (39)$$

where $f(x)$ is a sigmoid function of the form,

$$f(x) = \frac{y_1 - y_0}{1 + e^{k(x-x_0)}} + y_0 \quad (40)$$

Second, we require the effect of assembly bias to be minimal at high masses, where there is no need to increase the clustering signal, and stronger at low masses. Similar to the model for scatter, we parametrize the strength of assembly bias, ρ , as a function of halo mass using the same functional form:

$$\rho(M_{\text{peak}}) = f(M_{\text{peak}}) \quad (41)$$

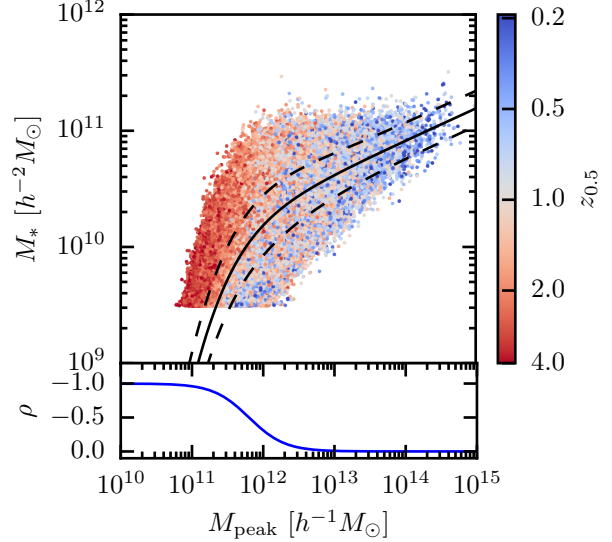


Figure 16. In the upper panel, we plot the SMHM relation for individual galaxies as points, colour-coded by the formation redshift, $z_{0.5}$. The mean relation is plotted as a solid line with the $\pm 1\sigma$ scatter shown as dashed lines. In the bottom panel, we show the strength of assembly bias, parametrized by the ρ parameter.

By trial and error, we find the parameters for eq. 39: $\log(x_0) = 12.0$, $y_1 = 0.3$, $y_0 = 0.15$, and $k = 2.0$, and the parameters for eq. 41: $\log(x_0) = 11.8$, $y_1 = -1.0$, $y_0 = 0.0$, and $k = 4.0$, provide a good fit to the SDSS galaxy clustering observations. The model for scatter is broadly within the scope of values found in other studies (shown as a black line in Fig. 15). The resulting SMHM relation in the RM model is shown in the top panel of Fig. 16, with the strength of the assembly bias effect on galaxies shown in the bottom panel.

The clustering signal in the RM model with assembly bias is shown in Fig. 17 along with the original RM model with no assembly bias effect. The model with assembly bias is much more consistent with galaxy clustering observations. In addition, the satellite fraction is very similar to the RV model. In a sense, the RM model with assembly bias is very similar to the RV model. The success of this scheme to fit clustering observations (and the RV model) suggests that assembly bias can increase the satellite fraction and therefore the clustering signal in SHAM models. However, neither of these models provide a *solution* to the clustering crisis. Neither self consistently model the evolution of the stellar mass function. Second, the formation redshift of sub-haloes is compared to host-haloes at $z = 0$, instead of other host-haloes at the time of accretion. In the next section, we attempt to self-consistently add assembly bias to the evolving SHAM models.

7.2 Evolving SHAM Assembly Bias

Given the success of our modifications to the RM model to introduce assembly bias to M_* , we now consider modifications to the evolving mass-based modes. As discussed, each

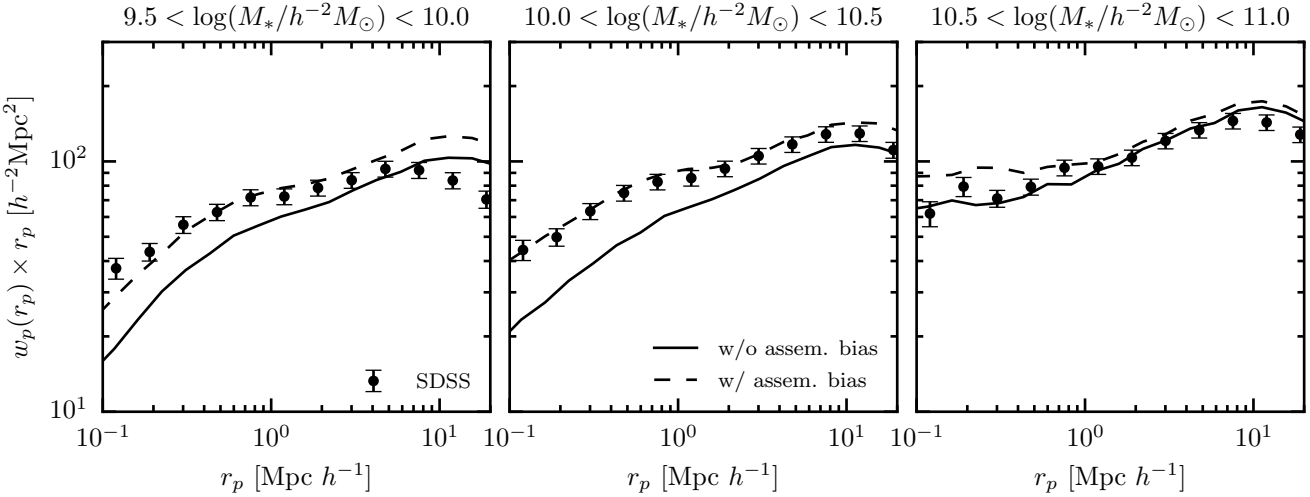


Figure 17. Similar to figure 3. The original RM model is shown as a solid line. The combined effect of including assembly bias with scatter in the SMHM relation in the RM model is shown as a dashed line.

of the evolving models makes the assumption that satellite galaxies at the time of accretion have the same mass as central galaxies in haloes with equal M_{peak} . In these models, correlating M_* with z_f will increase the mass of satellite galaxies if haloes which become sub-haloes form significantly earlier than haloes which remain host-haloes. This differs from the model for post-accretion satellite growth discussed in §6. In this model, galaxies which become satellites grow more quickly than galaxies which remain centrals. Therefore, satellites are “over-massive” compared to centrals at z_{acc} .

For the evolving models we adopt the same scatter model used for the RM model as described above. Instead of applying the CAM method at only $z = 0$, we apply it at each snapshot, z_{snap} , of the simulation, storing the M_* assigned to satellites that were just accreted, i.e. $z_{\text{acc}} = z_{\text{snap}}$. In this way, the formation time of satellites is compared to host-haloes at z_{acc} . After z_{acc} , satellites are assumed to not grow further. This is accomplished in a computationally efficient manner as follows. For each (sub-)halo, we compare its formation time, z_f , to the full $p(z_f|M_{\text{peak}}, z_{\text{acc}})$ of all host-haloes of equivalent mass at the redshift of accretion (for host haloes we set $z_{\text{acc}} = 0$) to find its associated percentile location in the distribution, p_f . We then assign stellar mass to (sub-)haloes by modifying eq. 25 such that the scatter is now correlated with z_f :

$$\log[M_*(M_{\text{peak}}, a_{\text{acc}})] = \log[\langle M_* | M_{\text{peak}} \rangle(a_{\text{acc}})] + \mathcal{F}^{-1}(0, \sigma_{\log(M_*)}, 1 - p_f) \quad (42)$$

where $\mathcal{F}^{-1}(0, \sigma_{\log(M_*)}, 1 - p_f)$ is the quantile function of a normal distribution with mean 0 and log-scatter $\sigma_{\log(M_*)}$. In this way, galaxies with earlier formation times are assigned larger stellar masses.

We find that no formation time parameter between $z_{0.1}$ and $z_{0.9}$ is sufficient to increase M_* of satellites enough to affect the clustering signal in each model substantially enough to fit the observed clustering signal. The earliest formation time we try in this model is $z_{0.1}$, which results in the weakest effect. The most recent we try is $z_{0.9}$, which results in the

strongest effect. However, even using $z_{0.9}$ only increases f_{sat} in the B13 and M13 models by only $\sim 2 - 3\%$, resulting in a minimal effect on galaxy clustering.

8 DISCUSSION & SUMMARY

We have shown that there is no published sub-halo abundance matching (SHAM) model that simultaneously:

- (i) fits the clustering of galaxies at $z=0$, $w_p(r_p)$,
- (ii) reproduces the evolution of the stellar mass function, $\phi(M_*, z)$,
- (iii) and uses only identified, extant, sub-haloes in high resolution dark matter simulations.

Models that fit observations of galaxy clustering are incompatible with the observed evolution of the stellar mass function and expectations for the build up of stellar mass in haloes. Conversely, SHAM models which self-consistently fit the stellar mass function as it evolves significantly under-predict galaxy clustering signals at small scales ($\leq 1 h^{-1} \text{Mpc}$). This tension exposes a clustering “crisis” for SHAM.

Of the five different models examined in this work, only SHAM based on rank ordering (sub-)haloes by peak maximum circular velocity, V_{peak} , (RV model) results in a robust galaxy clustering signal consistent with observations. This finding is in-line with previous work that finds V_{peak} is the best quantity to consider when fitting galaxy clustering observations (Reddick et al. 2013; Lehmann et al. 2015). However, an implicit assumption in V_{peak} SHAM is that the stellar mass- V_{peak} (SMVP) relation does not evolve. Because haloes grow their potential wells early (e.g. van den Bosch et al. 2014), a non-evolving SMVP relation results in haloes building up stellar mass too early.

SHAM models based on peak halo mass, M_{peak} , (RM, M13, B13, and Y12 models) do not produce strong enough clustering signals with respect to observations, especially on small scales. Evolving models like M13, B13, Y12, and more

recently by Rodríguez-Puebla et al. (2017), have been used to learn about the star-formation history of galaxies, quenching physics, and the contribution of merging to the build up of galaxies and stellar haloes with significant success. Given the wide-ranging utility of these models, we have examined three modifications to mass-based SHAM models that alleviate the clustering crisis to varying degrees: the addition of orphan galaxies, stellar mass growth post-accretion for satellites, and assembly bias. Each of these “solutions” addresses the clustering crisis by increasing the number of satellite galaxies.

This tension between fitting clustering observations and abundance of satellites is what drives the demand for increasing the number of satellites in many other studies. For example, in the original semi-analytic implementation of the Y12 model, Yang et al. (2012) find a need for more massive satellites and longer sub-halo survival times than traditional SHAM implementations. It is only when we apply the Y12 model to dark matter simulations directly, that it becomes clear that there are not enough extant sub-haloes to fit clustering observations. Lim et al. (2016) find a similar result when fitting the conditional stellar mass function (CSMF), i.e. satellite abundances. Only models which allow for a significant orphan population can provide a good fit to the faint end of the CSMF, another indication that the true culprit in the clustering crisis is a lack of satellite galaxies. Furthermore, this problem is not unique to SHAM models. Pujol et al. (2017), in a comparison of many galaxy formation models, find that only models with orphan galaxies are able to fit clustering observations on small scales.

While the need for orphan galaxies is well established, the motivation for the missing sub-haloes associated with orphan galaxies in high resolution simulations is lacking. While the mass resolution of simulations places an absolute limit on their ability to resolve highly stripped sub-haloes (no structures can exist below the particle mass, m_p), we find no empirical evidence of sufficiently massive missing sub-haloes. By examining the power-law behaviour of the sub-halo fraction, we find that the resolution of the Bolshoi simulation, $m_p = 1.35 \times 10^8 h^{-1} M_\odot$, appears to be sufficient to model SDSS-like galaxy samples ($M_* \geq h^{-2} M_\odot$), where the majority of satellite galaxies live in haloes with peak masses $\gtrsim 1000 \times m_p$. This finding is consistent with an independent analysis based on the convergence of the galaxy clustering signal (Guo & White 2013) from SHAM models. Despite the lack of evidence for large numbers of missing sub-haloes, we find that mass-based SHAM models require that approximately half of all satellite galaxies are orphans in order to fit galaxy clustering observations. This large fraction of orphan galaxies is similar to the number required by Yang et al. (2012).

Regardless, the appeal of SHAM is based on its ability to leverage the statistical power of large, cosmological, dark matter only (DMO) simulations. If DMO simulations are not able to resolve substructure abundance to within a factor of ~ 2 , the utility of SHAM becomes questionable. Furthermore, DMO simulations may not be reliable probes of substructure if the presence of baryons and various astrophysical processes associated with galaxy evolution significantly modify the abundance, distribution, and structure of sub-haloes. For example, the inclusion of baryons in cosmological simulations may more tightly bind sub-haloes, there-

fore increasing the survival time and abundance (Fiacconi et al. 2016). However, the net effect of baryonic physics on sub-haloes is not well understood. Despali & Vegetti (2016) find that the abundance of sub-haloes with peak mass $\sim 10^{10} h^{-1} M_\odot$ is increased in the EAGLE simulation (Schaye et al. 2015), while it is decreased in the Illustris simulation (Vogelsberger et al. 2014). An enhanced destruction of dwarf galaxy mass sub-haloes ($10^5 - 10^{10} h^{-1} M_\odot$) has been found in many zoom-in simulations (Read et al. 2006a,b; Brooks & Zolotov 2014; Wetzel et al. 2016). Garrison-Kimmel et al. (2017) find that the tidal field of central galaxies’ disks results in a depletion in the abundance of sub-haloes by a factor of ~ 2 in the central regions compared to DMO simulations. If the inclusion of the baryonic physics of galaxy formation and evolution generically decreases the abundance of sub-haloes, this only serves to increase the small scale galaxy clustering problem in SHAM.

Given the uncertain contribution of orphan galaxies, in this paper we have also examined two other physically motivated methods to enhance the satellite contribution in mass-based SHAM models. First, we examine the effect of allowing satellite galaxies to grow in mass after accretion for some time before quenching. Within this framework, the process(es) which quenches satellites is delayed, while in the interim satellites continue to form stars similarly to central galaxies (Wetzel et al. 2013). This idea is at odds with the assumption in many SHAM models that the stellar mass of satellites is set at z_{acc} and serves as a sort of fossil record of the SMHM relation at that redshift. Continued growth after accretion generally increases the number of satellites above a given stellar mass threshold. We find that reasonable delay times before quenching result in modest increases to the satellite fraction and, as a result, the clustering signal on small scales. Again, Y12 find evidence for significant post-accretion evolution of stellar mass, such that satellites acquire a stellar mass that is close to that of central galaxies. Our model for growth allows for even larger masses, but remains insufficient. Behroozi et al. (2015) apply a similar model for post-accretion growth and find consistent results when examining close galaxy pairs, but do not comment on galaxy clustering. Regardless, our results suggest post-accretion evolution of satellites is an important phenomena to model in order to reproduce the small scale clustering of galaxies, but this effect on its own is not sufficient to solve the clustering crisis in this paper.

Finally, we show that galaxy assembly bias can increase clustering in mass-based SHAM models. The increased clustering signal in V_{peak} -based SHAM is a result of assembly bias (Zentner et al. 2014; Mao et al. 2015). Using the CAM technique, we show that M_{peak} -based SHAM can produce similar results if it assumed that stellar mass is correlated with halo formation time at fixed M_{peak} . We find that such a model must contain two features. First, the strength of the galaxy assembly bias must decrease in high mass haloes. Second, the scatter in the SMHM relation must increase towards lower masses. M_{peak} -based SHAM with assembly bias explicitly added appears very similar to V_{peak} -based SHAM; however, neither model offers a consistent picture of how (sub-)haloes build stellar mass. As a result, this is not a complete solution to the crisis in this paper.

The ability of rank order SHAM models to fit galaxy clustering observations when galaxies are affected by assem-

bly bias motivates the construction of self-consistent evolving SHAM models with a similar assembly bias effect. In such a model, we assume that galaxies which become satellites grow more massive by the time they are accreted, after which time no further growth occurs. By correlating stellar mass and formation time at the time of accretion for satellites at every redshift output in the simulation, we compare the formation time of sub-haloes that were just accreted to all other host-haloes. Unfortunately, the difference between the formation time of sub-haloes and host-haloes when measured in this way is significantly smaller than when all $z = 0$ sub-haloes are compared to all host-haloes at $z = 0$ as was done in the rank order SHAM model with assembly bias. As a result, the effect of assembly bias is much smaller, and the evolving models with assembly bias continue to predict clustering signals that are too weak.

Regardless of the method, satellite galaxies at $z=0$ must be more massive than central galaxies in haloes of equal peak mass to match observations. Matching the detailed or even aggregate stellar mass growth history of both central and satellite galaxies may be beyond simple one (or two parameter) SHAM (CAM) models. We speculate that a combination of both continued stellar mass growth after accretion of satellites and galaxy assembly bias are necessary to resolve this crisis.

ACKNOWLEDGEMENTS

FvdB is supported by the Klaus Tschira Foundation and by the US National Science Foundation through grant AST 1516962.

NP is supported in part by DOE DE-SC0008080

REFERENCES

- Baldry I. K., Glazebrook K., Driver S. P., 2008, MNRAS, 388, 945
- Behroozi P. S., Conroy C., Wechsler R. H., 2010, ApJ, 717, 379
- Behroozi P. S., Wechsler R. H., Wu H.-Y., 2013a, ApJ, 762, 109
- Behroozi P. S., Wechsler R. H., Wu H.-Y., Busha M. T., Klypin A. A., Primack J. R., 2013b, ApJ, 763, 18
- Behroozi P. S., Wechsler R. H., Conroy C., 2013c, ApJ, 770, 57
- Behroozi P. S., Wechsler R. H., Lu Y., Hahn O., Busha M. T., Klypin A., Primack J. R., 2014a, ApJ, 787, 156
- Behroozi P. S., Wechsler R. H., Lu Y., Hahn O., Busha M. T., Klypin A., Primack J. R., 2014b, ApJ, 787, 156
- Behroozi P. S., et al., 2015
- Bell E. F., McIntosh D. H., Katz N., Weinberg M. D., 2003, ApJS, 149, 289
- Bell E. F., et al., 2005, ApJ, 625, 23
- Blanton M. R., Roweis S., 2007, AJ, 133, 734
- Borch A., et al., 2006, A&A, 453, 869
- Brooks A. M., Zolotov A., 2014, ApJ, 786, 87
- Bryan G. L., Norman M. L., 1998, ApJ, 495, 80
- Bundy K., et al., 2006, ApJ, 651, 120
- Carlberg R. G., 1994, ApJ, 433, 468
- Chabrier G., 2003, The Publications of the Astronomical Society of the Pacific, 115, 763
- Conroy C., Wechsler R. H., 2009, ApJ, 696, 620
- Conroy C., Wechsler R. H., Kravtsov A. V., 2006, ApJ, 647, 201
- Desmond H., Wechsler R. H., 2015, MNRAS, 454, 322
- Despali G., Vegetti S., 2016, arXiv, p. arXiv:1608.06938
- Diemer B., Sparre M., Abramson L. E., Torrey P., 2017, ApJ, 839, 26
- Fall S. M., Efstathiou G., 1980, MNRAS, 193, 189
- Fiacconi D., Madau P., Potter D., Stadel J., 2016, ApJ, 824, 144
- Gao L., White S. D. M., 2007, Monthly Notices of the Royal Astronomical Society: Letters, 377, L5
- Gao L., Springel V., White S. D. M., 2005, Monthly Notices of the Royal Astronomical Society: Letters, 363, L66
- Garrison-Kimmel S., et al., 2017, arXiv, p. arXiv:1701.03792
- Gill S. P. D., Knebe A., Gibson B. K., 2005, MNRAS, 356, 1327
- Guo Q., White S., 2013, MNRAS, 437, 3228
- Guo Q., Guo Q., White S., White S., Li C., Boylan-Kolchin M., 2010, MNRAS, 404, 1111
- Hearin A. P., Watson D. F., 2013, MNRAS, 435, 1313
- Hearin A. P., Zentner A. R., Berlind A. A., Newman J. A., 2013, MNRAS, 433, 659
- Hearin A. P., Watson D. F., Becker M. R., Reyes R., Berlind A. A., Zentner A. R., 2014, MNRAS, 444, 729
- Hearin A., et al., 2016
- Hu W., Kravtsov A. V., 2003, ApJ, 584, 702
- Jiang F., van den Bosch F. C., 2016, MNRAS, 458, 2848
- Jimenez R., Panter B., Heavens A. F., Verde L., 2005, MNRAS, 356, 495
- Juneau S., et al., 2005, ApJ, 619, L135
- Klypin A. A., Trujillo-Gomez S., Primack J., 2011, ApJ, 740, 102
- Knebe A., et al., 2011, MNRAS, 415, 2293
- Knebe A., et al., 2013, MNRAS, 435, 1618
- Kodama T., et al., 2004, MNRAS, 350, 1005
- Kravtsov A. V., Klypin A. A., Khokhlov A. M., 1997, ApJS, 111, 73
- Kravtsov A. V., Berlind A. A., Wechsler R. H., Klypin A. A., Gottlöber S., Allgood B., Primack J. R., 2004, ApJ, 609, 35
- Kroupa P., 2001, MNRAS, 322, 231
- Lehmann B. V., Mao Y.-Y., Becker M. R., Skillman S. W., Wechsler R. H., 2015
- Li C., White S. D. M., 2009, MNRAS, 398, 2177
- Li Y., Mo H. J., Gao L., 2008, MNRAS, 389, 1419
- Lim S., Mo H., Lan T.-W., Ménard B., 2016
- Lin W. P., Jing Y. P., Lin L., 2003, MNRAS, 344, 1327
- Ludlow A. D., Navarro J. F., Springel V., Jenkins A., Frenk C. S., Helmi A., 2009, ApJ, 692, 931
- Macciò A. V., Kang X., Fontanot F., Somerville R. S., Koposov S. E., Monaco P., 2009, MNRAS, pp 1995–2008
- Mamon G. A., Sanchis T., Salvador-Solé E., Solanes J. M., 2004, A&A, 414, 445
- Mandelbaum R., Wang W., Zu Y., White S., Henriques B., More S., 2015
- Mao Y.-Y., Williamson M., Wechsler R. H., 2015, ApJ, 810, 21
- Matthee J., Schaye J., Crain R. A., Schaller M., Bower R., Theuns T., 2016
- More S., van den Bosch F. C., Cacciato M., Mo H. J., Yang X., Li R., Li R., 2009, MNRAS, 392, 801
- More S., van den Bosch F. C., Cacciato M., Skibba R., Mo H. J., Yang X., 2011, MNRAS, 410, 210
- Moster B. P., Somerville R. S., Maulbetsch C., van den Bosch F. C., Macciò A. V., Naab T., Oser L., 2010, ApJ, 710, 903
- Moster B. P., Naab T., White S. D. M., 2013, MNRAS, 428, 3121
- Moustakas J., et al., 2013, ApJ, p. 50
- Muldrew S. I., Pearce F. R., Power C., 2011, MNRAS, 410, 2617
- Navarro J. F., Frenk C. S., White S. D. M., 1997, 490, 493
- Neistein E., van den Bosch F. C., Dekel A., 2006, MNRAS, 372, 933
- Onions J., et al., 2012, MNRAS, 423, 1200
- Padmanabhan N., White M., Eisenstein D. J., 2007, MNRAS, 376, 1702
- Paranjape A., Kovač K., Hartley W. G., Pahwa I., 2015
- Pujol A., et al., 2017, arXiv, p. arXiv:1702.02620

- 1405 Read J. I., Wilkinson M. I., Evans N. W., Gilmore G., Kleyna 1468
 1406 J. T., 2006a, MNRAS, 366, 429
 1407 Read J. I., Wilkinson M. I., Evans N. W., Gilmore G., Kleyna 1469
 1408 J. T., 2006b, MNRAS, 367, 387
 1409 Reddick R. M., Wechsler R. H., Tinker J. L., Behroozi P. S., 2013, 1471
 1410 ApJ, 771, 30
 1411 Rees M. J., Ostriker J. P., 1977, MNRAS, 179, 541
 1412 Rodríguez-Puebla A., Primack J. R., Avila-Reese V., Faber S. M., 1474
 1413 2017, arXiv, p. arXiv:1703.04542
 1414 Saito S., et al., 2015
 1415 Sales L. V., Navarro J. F., Abadi M. G., Steinmetz M., 2007, 1477
 1416 MNRAS, 379, 1475
 1417 Schaye J., et al., 2015, MNRAS, 446, 521
 1418 Sunayama T., Hearin A. P., Padmanabhan N., Leauthaud A., 1479
 1419 2015
 1420 The Astropy Collaboration et al., 2013, A&A, 558, A33
 1421 Tinker J. L., et al., 2016
 1422 Tomczak A. R., et al., 2014, ApJ, 783, 85
 1423 Vale A., Ostriker J. P., 2004, MNRAS, 353, 189
 1424 Vogelsberger M., et al., 2014, MNRAS, 444, 1518
 1425 Wang L., Jing Y. P., 2010, MNRAS, 402, 1796
 1426 Wang L., Li C., Kauffmann G., De Lucia G., 2006, MNRAS, 371, 1485
 1427 537
 1428 Watson D. F., Berlind A. A., Zentner A. R., 2012, ApJ, 754, 90
 1429 Watson D. F., et al., 2015, MNRAS, 446, 651
 1430 Wechsler R. H., Bullock J. S., Primack J. R., Kravtsov A. V., 1481
 1431 Dekel A., 2002, ApJ, 568, 52
 1432 Wechsler R. H., Zentner A. R., Bullock J. S., Kravtsov A. V., 1486
 1433 Allgood B., 2006, ApJ, 652, 71
 1434 Wetzel A. R., White M., 2010, MNRAS, 403, 1072
 1435 Wetzel A. R., Tinker J. L., Conroy C., 2012, MNRAS, 424, 232
 1436 Wetzel A. R., Tinker J. L., Conroy C., van den Bosch F. C., 2013, 1488
 1437 MNRAS, 432, 336
 1438 Wetzel A. R., Tinker J. L., Conroy C., van den Bosch F. C., 2014, 1490
 1439 MNRAS, 439, 2687
 1440 Wetzel A. R., Hopkins P. F., Kim J.-h., Faucher-Giguere C.-A., 1491
 1441 Kereš D., Quataert E., 2016, ApJ, p. L23
 1442 White S. D. M., Rees M. J., 1978, MNRAS, 183, 341
 1443 Yang X., Mo H. J., van den Bosch F. C., 2003, MNRAS, 339, 1494
 1444 1057
 1445 Yang X., Mo H. J., van den Bosch F. C., Zhang Y., Han J., 2012, 1496
 1446 ApJ, 752, 41
 1447 Yang X., Mo H. J., van den Bosch F. C., Bonaca A., Li S., Lu Y., 1498
 1448 Lu Y., Lu Z., 2013, ApJ, 770, 115
 1449 Zentner A. R., Hearin A. P., van den Bosch F. C., 2014, MNRAS, 1500
 1450 443, 3044
 1451 Zu Y., Mandelbaum R., 2015b
 1452 Zu Y., Mandelbaum R., 2015a
 1453 van Kampen E., 1995, MNRAS, 273, 295
 1454 van Uitert E., et al., 2016, MNRAS, 459, 3251
 1455 van den Bosch F. C., Jiang F., 2014
 1456 van den Bosch F. C., Jiang F., 2016, MNRAS, 458, 2870
 1457 van den Bosch F. C., Yang X., Mo H. J., 2003, MNRAS, 340, 771
 1458 van den Bosch F. C., et al., 2007, MNRAS, 376, 841
 1459 van den Bosch F. C., Aquino D., Yang X., Mo H. J., Pasquali A., 1507
 1460 McIntosh D. H., Weinmann S. M., Kang X., 2008, MNRAS, 1508
 1461 387, 79
 1462 van den Bosch F. C., More S., Cacciato M., Mo H., Yang X., 2013, 1510
 1463 MNRAS, 430, 725
 1464 van den Bosch F. C., Jiang F., Hearin A., Campbell D., Watson 1512
 1465 D., Padmanabhan N., 2014, MNRAS, 445, 1713
 1466 van den Bosch F. C., Jiang F., Campbell D., Behroozi P., 2016, 1513
 1467 MNRAS, 455, 158

APPENDIX A: HALO PROPERTIES

In this section we describe how we calculate properties for (sub-)haloes which depend on their growth history. We use the merger trees constructed using the **Consistent** trees algorithm (Behroozi et al. 2013b) built on the **ROCKSTAR** halo catalogues from the Bolshoi simulation. We distinguish between host-haloes and sub-haloes using the **upid** tag for each halo. If **upid** $\equiv -1$, a halo is considered a host; otherwise, if **upid** > 0 , we consider it a sub-halo. For this work, we do not distinguish between higher order sub-haloes (i.e. sub-sub-haloes).

A1 Peak Halo Mass

We use the peak halo mass obtained by each (sub-)halo to assign stellar mass in each of the models discussed in this paper. We calculate the peak mass, \tilde{M}_{peak} , a (sub-)halo at $z=0$ obtained throughout its history while not identified as a sub-halo as:

$$\tilde{M}_{\text{peak}} = \text{MAX}[m'_{\text{vir}}(z)] \quad (\text{A1})$$

where,

$$m'_{\text{vir}}(z) = \begin{cases} m_{\text{vir}}(z) & \text{if host-halo at } z \\ 0.0 & \text{if sub-halo at } z \end{cases} \quad (\text{A2})$$

We then define z_{peak} as the redshift where $m'_{\text{vir}}(z_{\text{peak}}) \equiv \tilde{M}_{\text{peak}}$. This differs from the typical definition of peak halo mass which does not require the peak mass to be obtained while a halo is identified as a host-halo:

$$M_{\text{peak}} = \text{MAX}[m_{\text{vir}}(z)] \quad (\text{A3})$$

The former definition, \tilde{M}_{peak} , disregards any mass growth which occurs while a halo is identified as a sub-halo. We prefer \tilde{M}_{peak} as a physical parameter because most growth that occurs while a halo is identified as a sub-halo is most often a numerical artifact. However, we do note that we ignore the rare case of subhalo-subhalo mergers. In Fig. A1 we show the growth histories for three haloes in the Bolshoi simulation. In each panel, we also show the running $\tilde{M}_{\text{peak}}(z)$ and mark the redshift where \tilde{M}_{peak} is reached. In the right hand panel we show a case where $\tilde{M}_{\text{peak}} \neq M_{\text{peak}}$ for a halo which briefly ‘grows’ in mass after accretion. We find this is the case for $\sim 10\%$ of sub-haloes.

A2 Halo Accretion Time

The purpose of this section is to define a “primary” accretion redshift, $z_{\text{acc,prim}}$, which is most important for galaxy evolution. Each of the evolving models in this work require a single accretion redshift for all sub-haloes, where it is assumed that the stellar mass of satellites is set at the time of accretion, or where a special post-accretion growth regime begins. However, a halo may undergo many accretion events throughout its history. This makes the identification of a single, most important, accretion redshift non-trivial.

With this in mind, we define the accretion redshift of a halo as the redshift at which it is first identified as a sub-halo after having been first identified as a host-halo⁷. Fur-

⁷ For the rare case of ‘immaculate’ sub-haloes, sub-haloes with

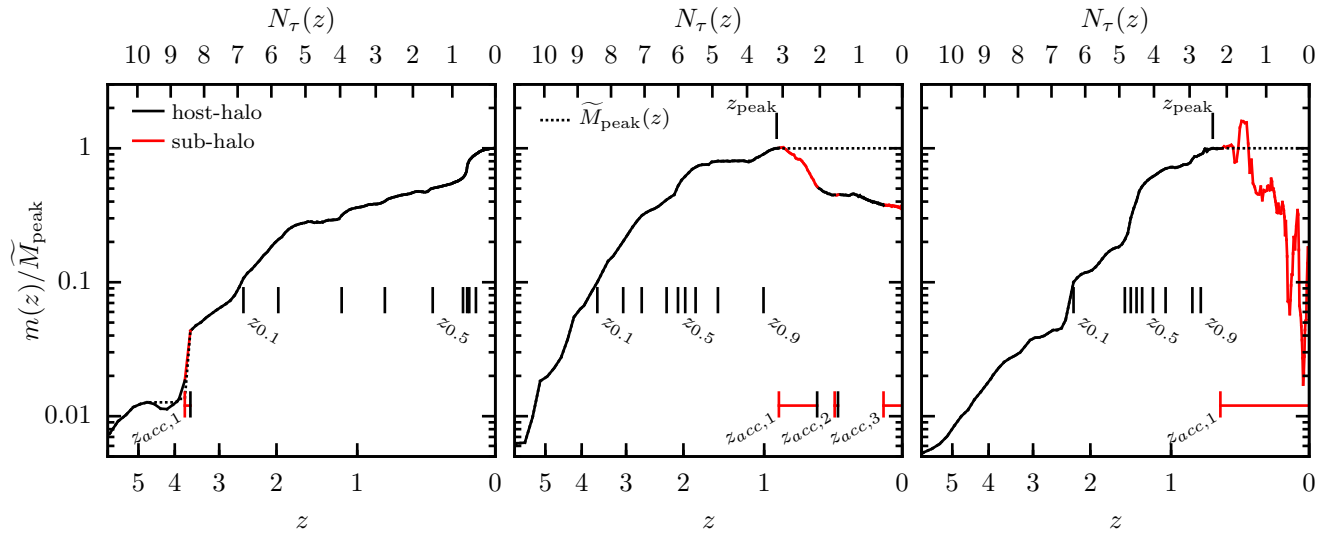


Figure A1. As an example, we show the mass growth histories for three haloes, all with a peak mass of $\sim 10^{12} h^{-1} M_\odot$. When a halo is identified as a host-halo ($\text{upid} \equiv -1$) $m_{\text{vir}}(z)/\tilde{M}_{\text{peak}}$ is shown as a solid black line. When a halo is identified as a sub-halo ($\text{upid} > 0$) $m_{\text{vir}}(z)/\tilde{M}_{\text{peak}}$ is shown as a solid red line. A series of formation times, $z_f = [0.1, 0.2, \dots, 0.9]$ are marked as vertical black dashes below the growth histories. Similarly, z_{peak} is marked above the growth histories. At the bottom of each panel, any accretion redshifts are shown as a red vertical dash connected to the associated ejection redshift marked with a black vertical dash (or through $z=0$ if it remains a sub-halo). The running peak mass, $\tilde{M}_{\text{peak}}(z)$, is plotted as a dotted black line. The upper x-axis in each panel is the number of dynamical times until $z=0$ from eq. A4.

thermore, because a sub-halo's orbit may take it beyond the virial radius of its host (e.g. backsplash haloes), it is possible to identify multiple accretion redshifts for many haloes. Given this, we define $z_{\text{acc},n}$ as the redshift a halo is identified as a sub-halo for the n^{th} time. We also tabulate 'ejection' redshifts, $z_{\text{ejet},n}$, the redshift a halo is identified as being a host-halo after previously having been identified as a sub-halo for the n^{th} time. As an example, in the middle panel of Fig. A1, we show the growth history of a halo which underwent three accretion events and two ejections since $z \sim 6$.

We explore four definitions for $z_{\text{acc,prim}}$:

- (i) the highest accretion redshift, $z_{\text{acc},1}$,
- (ii) the most recent $z_{\text{acc},n}$,
- (iii) the highest accretion redshift that is not followed by a continuous period of more than two dynamical times as a host-halo before being re-accreted (or reaching $z=0$),
- (iv) and the highest accretion redshift that occurs after z_{peak} .

The first definition for $z_{\text{acc,prim}}$ we examine is $z_{\text{acc},1}$. We can eliminate this as a viable definition because we find that a significant fraction of host-haloes at $z \sim 0$ were briefly identified as a sub-halo at high redshifts. An example is shown in the left hand panel of Fig. A1. We find that between 4% and 10% of haloes more massive than $10^{12} h^{-1} M_\odot$ have $z_{\text{acc},1}$ and $z_{\text{ejt},1} > 3$ and remain a host-halo up to $z \sim 0$. It is clear that these haloes should be treated more as traditional host haloes than haloes that host satellite galaxies.

no progenitor (?), we use the first redshift for which the halo is identified.

The second definition we consider for $z_{\text{acc,prim}}$ is the most recent accretion redshift. This definition suffers the same problem as the previous by assigning too many host-haloes a high redshift $z_{\text{acc,prim}}$. In addition, such a definition ignores the accretion history of backsplash haloes by only considering the most recent accretion event. Up to 60% of sub-haloes are on orbits whose apocenter is beyond the virial radius of their effective host-halo, and around $\sim 10\%$ of accreted sub-structure is found beyond the virial radius of their associated host-halo at $z \sim 0$ (Lin et al. 2003; Gill et al. 2005; Sales et al. 2007; Ludlow et al. 2009; Wetzel et al. 2014; ?). The middle panel of Fig. A1 shows an example of a halo which was accreted and ejected multiple times in line with the expectation for backsplash haloes.

To address both spurious high-redshift accretions and backsplash haloes at lower redshift, we consider a third definition for $z_{\text{acc,prim}}$ that takes into account the amount of time a halo remains a host-halo after being ejected. For backsplash haloes, the time-scale for re-accretion will be on the order of dynamical time. If a halo remains a host-halo for much more time, evolution as a typical host-halo is more likely as in the case of host-haloes which were briefly identified as a sub-halo at high-redshift.

To this end, we calculate the number of dynamical times elapsed between redshift z and 0 as:

$$N_\tau(z) = \int_0^{t(z)} \frac{dt}{\tau_{\text{dyn}}(t)} \quad (\text{A4})$$

where τ_{dyn} is the dynamical time given by:

$$\begin{aligned}\tau_{\text{dyn}}(t) &= \sqrt{\frac{3\pi}{16G\bar{\rho}_h(z)}} \\ &= 1.628 h^{-1} \text{Gyr} \left[\frac{\Delta_{\text{vir}}(z)}{178} \right] \left[\frac{H(z)}{H_0} \right]^{-1}\end{aligned}\quad (\text{A5})$$

where $\bar{\rho}_h(z)$ is the average density of a virialized dark matter halo at redshift z . The number of dynamical times between the i^{th} ejection and the $i+1^{\text{th}}$ accretion is then given by:

$$\Delta N_\tau = N_\tau(z_{\text{ejt},i}) - N_\tau(z_{\text{acc},i+1}) \quad (\text{A6})$$

For any accretion redshift which is not followed by a continuous time, ΔN_τ , as a host-halo, we mark as the primary accretion redshift. For haloes that remain a host for ΔN_τ after being ejected, we disregard the previous accretion events when defining $z_{\text{acc,prim}}$. We find that $\Delta N_\tau = 2$ is a good threshold to separate backsplash-ing sub-haloes and host-haloes with spurious high redshift accretion events.

The final definition for the primary accretion redshift we explore is the highest redshift accretion that occurs after \bar{M}_{peak} . This naturally removes any prior accretion events that were followed by mass growth while also generally picking out the initial accretion redshift for haloes that backsplash. This definition lines up with $z_{\text{acc},1}$ in the middle and right-hand panels of Fig. A1. We also find that $z_{\text{acc,prim}}$ defined using the last two definitions (iii, iv) are different in less than 2% of haloes with mass greater than $10^{12} h^{-1} M_\odot$. Given the simplicity of this definition, we adopt this as our fiducial $z_{\text{acc,prim}}$ in the rest of this paper and simply refer to it as z_{acc} .

We show the effect on clustering for different definitions of $z_{\text{acc,prim}}$ for the M13 model in Fig. A2. The only significant difference is between the last accretion redshift (definition ii) and the others (i, iii, iv). Using the last accretion redshift results in satellites with larger stellar masses relative to the other definitions as a result of the evolution in the SMHM relation towards larger stellar masses at fixed halo mass as $z \rightarrow 0$. Satellites that are ejected get a boost in stellar mass relative to those that remain satellites. We consider this an unappealing model for satellite evolution.

A3 Halo Formation Time

We calculate the formation time of a halo, z_f , as the redshift at which a halo is first identified as exceeding a mass larger than or equal to $f \times \bar{M}_{\text{peak}}$ while not identified as a sub-halo. In Fig. A1 we show z_f for $f=0.1, 0.2, \dots, 0.9$ for three different halo growth histories marked with short vertical dashes below $m_{\text{vir}}(z)$ in each panel.

APPENDIX B: STELLAR MASS CONVERSIONS

Each of the evolving models in this paper (M13, B13, and Y12) was tuned to fit stellar mass functions based on different methods to measure M_* . In order to facilitate comparisons between models, we apply a set of simple conversion to correct for the mean difference in order to make the stellar masses more consistent with the Blanton & Roweis (2007)

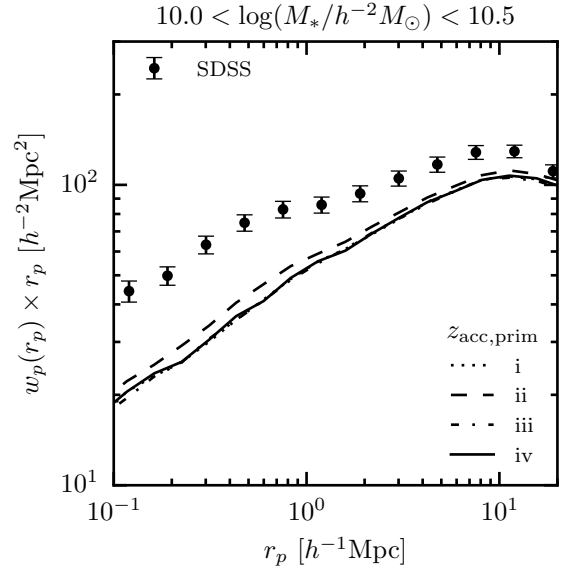


Figure A2. Similar to Fig. 12, a comparison of the effect of different definitions of $z_{\text{acc,prim}}$ on $w_p(r_p)$ in the M13 model. The model predictions for different $z_{\text{acc,prim}}$ definitions are shown as lines of various styles corresponding to the definitions listed in Appendix A2. The lines for definitions i, iii, and iv fall nearly on-top of each other.

stellar masses, M_{Blanton} , used in LW09 and the RM and RV models. A summary of these functions is shown in Fig. B1.

Here we describe in detail each of these conversions. M13 fits to the LW09 stellar mass function at $z \sim 0$ which was modified based on a conversion suggested by Guo et al. (2010) which transforms the stellar masses based on the SDSS r-band Petrosian magnitudes to ones based on SDSS r-band model magnitudes. We undo this modification by reducing the stellar masses in M13 by 10%. B13 fits to the Baldry et al. (2008) and Moustakas et al. (2013) mass functions at $z < 0.2$. The Baldry et al. (2008) stellar masses are an average of many different techniques which makes a simple conversion prescription difficult. On the other hand, Moustakas et al. (2013) provide a comparison between masses derived using the iSEDfit and the Blanton & Roweis (2007) masses. We find the the mean difference is well fit by:

$$\log(M_{\text{Blanton}}/M_{\text{iSEDfit}}) = a_1 + a_2 \tanh\left(\frac{M_{\text{iSEDfit}} - a_3}{a_4}\right) \quad (\text{B1})$$

where $a_1 = 0.0056$, $a_2 = -0.098$, $a_3 = 10.53$, and $a_4 = 0.82$. We transform the B13 masses using this relation and find satisfactory results. The Y12 model uses stellar masses based on the technique of Bell et al. (2003) assuming a universal IMF (Kroupa 2001; Borch et al. 2006). We use the inverse of the transformation between Bell et al. (2003) and Blanton & Roweis (2007) masses provided in Appendix A in LW09:

$$\begin{aligned}\log(M_{\text{Bell}}/M_{\text{Blanton}}) &= a_1 + a_2 M_{\text{Blanton}} + a_3 M_{\text{Blanton}}^2 \\ &\quad + a_3 M_{\text{Blanton}}^3 + a_3 M_{\text{Blanton}}^4\end{aligned} \quad (\text{B2})$$

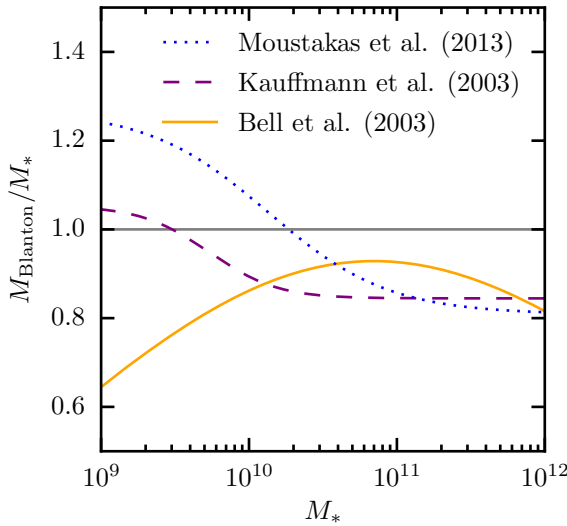


Figure B1. mass conversion between Blanton stellar masses and the other stellar mass systems used in this paper.

where $a_1 = 2.0$, $a_2 = -0.043$, $a_3 = -0.045$, $a_4 = 0.0032$, and $a_5 = -2.1 \times 10^{-5}$.

host. When a particle can be assigned to more than one host under this condition, we assign the particle to the nearest host-halo. After this process, we find that $\sim 1\%$ of clones occupy a host-halo with no associated particles (in our down-sampled catalogue). In this small fraction of cases, we revert to the first method.

Each of these methods has merits. The first method acts under the assumption that the sub-haloes that host orphan galaxies (and missing from the available halo catalogues) are a fair sampling of all sub-haloes. These clones will have the same radial profile as typical sub-haloes within host-haloes of equivalent mass. The second method results in a more centrally concentrated population of orphans, one that also naturally follows the shape of the host-halo. This may be a more appropriate if the majority of orphans occupy sub-haloes that are missing because they are hard to identify in the dense central regions of host-haloes or highly evolved sub-haloes which have sunk to the central regions of their host-halo. Neither of these methods will preserve sub-halo-sub-halo correlations. In particular, neither of these methods specifically deals with higher-order sub-haloes, e.g. sub-sub-haloes, and treats all sub-haloes regardless of order the same in the cloning process. To help with visualization of each of these methods, we plot the position of sub-haloes and clones in Fig. C1 for both methods. In the bottom panel, one can see that the clones are more centrally concentrated than both the extant sub-haloes and clones assigned positions maintaining the relative distance to the host-halo centre.

APPENDIX C: ORPHAN GALAXIES

We define “orphan” galaxies as satellites in our mock galaxy catalogues which have no identified sub-halo. Our implementation of abundance matching requires a halo or sub-halo be associated with each galaxy. In order to add the flexibility of including a population of orphan galaxies, we post-process the halo catalogues, adding “clone” sub-haloes that are made available to host orphan galaxies.

To generate a clone, we randomly draw from the list of all sub-haloes to choose a “donor” sub-halo. The clone sub-halo receives all the properties of the donor sub-halo (e.g. z_{acc}) except its phase space coordinates and those properties associated with its host-halo. A new host-halo is chosen for the clone by randomly choosing a host-halo with a mass close to that of the donor’s host (± 0.1 dex). We apply two methods to assign a new set of phase space coordinates to the clone:

(i) maintaining the relative position, $\Delta\vec{x}$, and velocity, $\Delta\vec{v}$, between a clone’s host-halo as in the donor’s host-halo (**sub-profile**),

(ii) assigning the phase-space coordinates of a randomly selected particle belonging to the clone’s host to the clone (**dm-profile**).

For the former method, we use the positions and velocities of host-haloes and sub-haloes from the ROCKSTAR halo catalogue. For the later, we use a down-sampled catalogue of dark matter particles consisting of $\sim 1\%$ of all particles to facilitate computational ease. We assign particles to host-haloes by finding all particles within a distance r_{vir} of each

APPENDIX D: DEGRADING RANK ORDER CORRELATIONS

Given two variables, X and Y , that form finite data sets, e.g. x_1, x_2, \dots, x_n , of length n , the correlation between the variables can be characterized by the Spearman’s rank order correlation coefficient:

$$\rho_{XY} = 1 - \frac{6 \sum d_i^2}{n(n^2 - 1)} \quad (\text{D1})$$

where d_i is the difference in ranks of x_i and y_i :

$$d_i = n_i^x - n_i^y \quad (\text{D2})$$

For example, if X and Y are both in rank order, e.g. $n_1^x = 1, n_2^x = 2, \dots, n_n^x = n$, then $\rho_{XY} = 1.0$.

Here we describe an algorithm to degrade the ordering of two variables, X and Y , each of length n . To begin with a positive correlation, each variable is placed in rank order:

$$\begin{aligned} X' &= \text{RANK}(X, X) \\ Y' &= \text{RANK}(Y, Y) \end{aligned} \quad (\text{D3})$$

where the $\text{RANK}(A, B)$ operator sorts A by the rank order values of B . It should be noted that to begin with a negative correlation between X and Y , X' would be put in inverse rank order, i.e. $X' = \text{RANK}(X, -X)$. Next, a new variable, Q , is calculated for X' from the ranks by adding a normal random variable to each rank:

$$q_i = n_i^{x'} + \mathcal{N}(0, \sigma_q \times n) \quad (\text{D4})$$

where σ_q is approximately the standard deviation of the

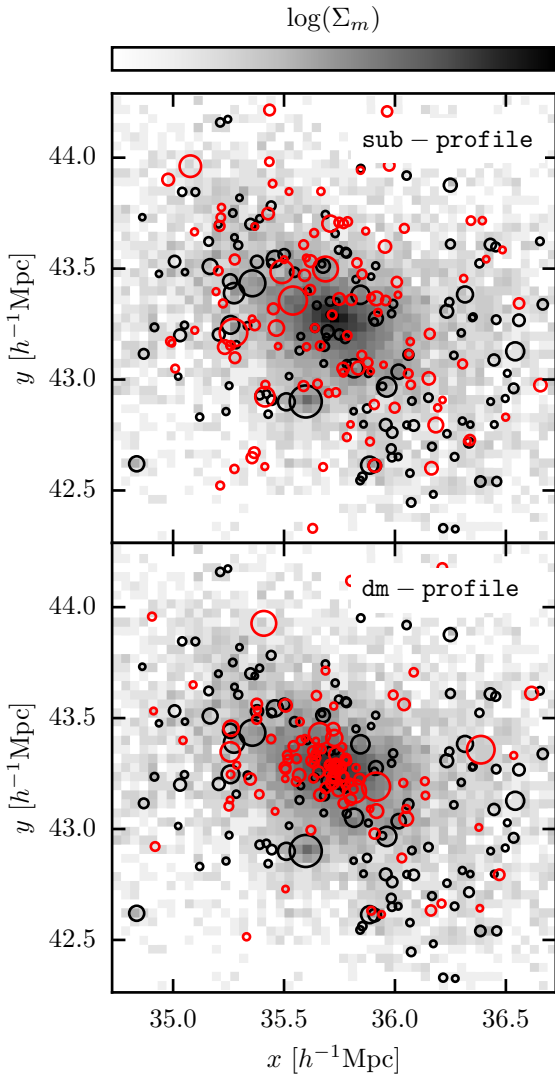


Figure C1. The projected distribution of sub-haloes with $M_{\text{peak}} > 10^{11} h^{-1} M_{\odot}$ (black circles) for an example host-halo ($m_{\text{vir}} \simeq 10^{14} h^{-1} M_{\odot}$), where the projected density of dark matter is shown in grey-scale (the same in upper and lower panels). In addition, the upper panel shows clone sub-haloes (red circles) where the relative distance and velocity with respect to the centre of mass is preserved (**sub-profile**). The bottom panel shows clone sub-haloes where the position and velocity is assigned by drawing random particles from the host-halo (**dm-profile**). The size of the circles is proportional to the viral radius at peak mass, $r_{\text{vir}}(z_{\text{peak}})$, of each sub-halo.

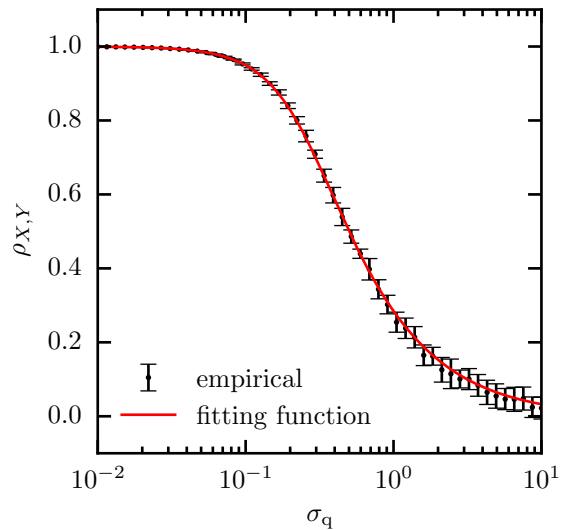


Figure D1. The relation between rank scatter parameter, σ_q , and the Spearman's correlation coefficient, ρ . The fitting function, eq. D6, is shown as a red line.

we examined the relation between the correlation coefficient, ρ_{XY} , and σ_q for two uniform random variables of length $n = 10^3$. For each value of σ_q we repeat the process described above 100 times. The error bars in Fig. D1 are the standard deviation in ρ_{XY} from these 100 realizations. From this, we derive the relation between $\langle \rho_{XY} \rangle$ and σ_q , and we use this relation to choose σ_q for a desired value of ρ_{XY} . We provide an accurate fitting function for the relation given by:

$$\langle \rho_{XY} \rangle(\sigma_q) = 1 - f(\sigma_q) \quad (\text{D6})$$

$$f(x) = \frac{1}{2} e^{-\left(\frac{x}{x_1}\right)^{\alpha}} + \frac{1}{2} \left[1 + \left(\frac{x}{x_2}\right)^{\beta} \right]^{-1}$$

where $x_1 = 2/3$, $x_2 = 0.3$, $\alpha = -1$, and $\beta = -2$. Furthermore, this relation is independent of the size of X and Y and is not affected by the distribution of values themselves since it is based on the rank ordering.

This paper has been typeset from a TeX/LaTeX file prepared by the author.

change in the order relative to the length of n . X' can then be re-ordered by Q :

$$X'' = \text{RANK}(X', Q) \quad (\text{D5})$$

Henceforth, we will refer to these two variables with transformed ordering simply as X and Y .

This method is inherently random in nature, and given a value of σ_q , the rank order correlation between X and Y will vary depending on the size of the data sets. In Fig. D1